

**THE FIRST STEP TO A FRAMEWORK FOR GAIT-TRAINING
WITH A BILATERAL APPROACH**

by

Duanyi Wei

A thesis submitted to the Faculty of the University of Delaware in partial fulfillment of the requirements for the degree of Master of Science in Mechanical Engineering

Fall 2018

© 2018 Duanyi Wei
All Rights Reserved

**THE FIRST STEP TO A FRAMEWORK FOR GAIT-TRAINING
WITH A BILATERAL APPROACH**

by

Duanyi Wei

Approved: _____
Jill Higginson, Ph.D.
Co-Chair on behalf of the Advisory Committee

Approved: _____
Ioannis Poulakakis, Ph.D.
Co-Chair on behalf of the Advisory Committee

Approved: _____
Ajay K. Prasad, Ph.D.
Chair of the Department of Mechanical Engineering

Approved: _____
Levi T. Thompson, Ph.D.
Dean of the College of Engineering

Approved: _____
Douglas J. Doren, Ph.D.
Interim Vice Provost for the Office of Graduate and Professional
Education

ACKNOWLEDGMENTS

First of all, I would like to thank my advisors - Prof. Poulakakis and Prof. Higginson - for having me as their student at the Robotic Locomotion Lab (RLL) and the Neuromuscular Biomechanics Lab (NBL). Their exceptional vision, knowledge, and passion have always been the caliber to what I tried to align myself with. I am very grateful for having two accomplished and caring advisors working with me through the journey. I would also like to thank my committee member Prof. Sergi, for his instrumental advice. It has been a great pleasure to work with some of great people from both labs. I thank Sushant, Anthony, Mohamad, Qu, Xin from RLL; Luke, Nicole, Hao-yuan, Brian, Kevin, Ana, Reza, Amy, Kelly from NBL; and Andrea and Andrew from Prof. Sergi's group, for their help and being such inspirations for me along the way.

Outside the lab, many people directly or indirectly contributed to my completion of this thesis. I would like to thank Jeff and Hasan for being such accommodating and amazing roommates over the years. I would thank Adam, Brian, Zach, Diana, Raja, Rohit and other fellows in the department for making my graduate life such a fun and vivid journey. I am very grateful for the great friendship I forged here in Delaware with Zhengyuan, Lan, and countless others whom I have the privilege to meet.

This thesis is a dedication to my family. I thank my grandparents and parents for always being supportive and proud of me. I thank my wife Aiyi for saying yes to spending rest of her life with me and her unwavering confidence in me.

TABLE OF CONTENTS

LIST OF TABLES	vi
LIST OF FIGURES	vii
ABSTRACT	x
 Chapter	
1 INTRODUCTION	1
1.1 Bilateral Coordination	1
1.2 Reductive Model	2
2 MODEL	6
2.1 Reduced-order Biped Model	6
2.1.1 Assisted-Leg Swing (AS) and Assisted-leg Impact (AI)	10
2.1.2 Double Stance (DS) and Unassisted-leg Liftoff (UL)	12
2.1.3 Unassisted-leg Swing (US) and Unassisted-leg Impact (UI)	15
2.1.4 Double Stance (DS) and Assisted-leg Liftoff (AL)	16
2.1.5 Summary of Model Dynamics	16
2.2 Periodic Gait Cycle and Poincaré Return Map	17
2.2.1 Periodic Solutions and Periodic Gait	18
2.2.2 Poincaré Return Map and Fixed Points	20
2.3 Walking Pattern Generation	22
2.3.1 Interlimb Coordination Strategy	23
2.3.2 Desired Coordination Patterns	27
2.3.3 Gait Parameters Optimization	29
2.4 Simulation Experiment	30
2.4.1 Set-point Control	30
2.4.2 Gait Stabilization	33
2.4.3 Speed Modulation	34
3 HUMAN EXPERIMENT	36
3.1 Research Design	36
3.2 Participant	36
3.3 Gait Evaluation	37

3.4	Data Analysis.....	38
4	RESULTS.....	40
4.1	Periodic Walking Gaits and Properties.....	40
4.2	Model Validation.....	42
4.3	Potency of Interlimb Coordination for Gait-training in Simulations	43
4.3.1	Scenario I: Gait Stabilization.....	43
4.3.2	Scenario II: Speed Modulation.....	44
4.4	Experimental Validation.....	48
5	DISCUSSION.....	50
5.1	Novelty of Model	50
5.2	Significance of Interlimb Coordination.....	51
5.3	Implications of Interlimb Coordination to Gait-training	52
5.4	Limitations.....	54
6	CONCLUSIONS AND FUTURE WORK.....	57
6.1	Conclusions	57
6.2	Future Work.....	58
6.2.1	Model Framework	58
6.2.2	Experimental Validation.....	59
	REFERENCES	61

LIST OF TABLES

Table 1:	Model and Subject Parameters	40
Table 2:	Kinematic Parameters from Simulation and Experimental Results	44

LIST OF FIGURES

Figure 1:	Reduced-order model of human locomotion. a) 4 degrees-of-freedom model with an asymmetric leg setup: the unassisted/affected side (red) and the two-link assisted/ affected side (black); model parameters (mass, length) of each segment are shown. b) two-link assisted leg model with joint torque at assisted hip (u_1) and assisted knee joints (u_2) that are coupled with gait variable (θ) during assisted-leg swing phase; Push-off effort by the unassisted-leg side at its liftoff is modeled as an impulse (δF_{UL}) along the unassisted leg. c) D-SLIP model with unassisted hip torque (u_3) during unassisted-leg swing. 4
Figure 2:	Continuous phases and transitional events of the gait cycle for the reduced-order biped model..... 7
Figure 3:	Geometric interpretation of a Poincaré return map $P: S \rightarrow S$ for a system with impulse effects. The switching surface S is selected to be the Poincaré section. The dashed line and solid line stand for the impact phase model and swing phase model, respectively. Δ is the impact map. $\varphi t, \Delta x$ is a solution of the continuous phase..... 19
Figure 4:	Evolution of the model during continuous phases and transition events and control schemes for each phases. The model is actuated during the swing phases (AS and US) by the joint torques (blue) that are coupled with gait progression variable θ . The model evolves along its intrinsic dynamics during the double stance phases. 24
Figure 5:	Schematics of the control objectives for the set-point controller and coordination controller 33
Figure 6:	Control diagram of push-off adaptive treadmill control 37
Figure 7:	a) An illustration of the integral of anterior-posterior component of ground reaction force (GRF) profile during the propulsive duration T_p . b) an illustration of IEPO as the projection of propulsive impulse along the unassisted-leg as the measurement of push-off impulse. 39

Figure 8:	Evolution of the hip vertical displacement (a), hip vertical velocity (b), hip forward displacement (c) and hip forward velocity (d) during one gait cycle. The vertical lines correspond to the events; from left to right: assisted-leg liftoff, assisted-leg impact, unassisted-leg liftoff and unassisted-leg impact. The torque profile for unassisted side joint (e) and assisted side joints (f) during the normalized swing phase of the corresponding side. In (f), the blue and green line correspond to the hip and knee torques, respectively.	41
Figure 9:	a) Joint kinematics of assisted-leg hip (blue) and knee (green) angle. The simulated joint angles (solid) and experimental joint outputs (dashed) are shown. The gait cycle starts at assisted leg impact and ends at assisted-leg swing just before impact, and the gait cycle is normalized. b) The mean and standard deviation of the GRF profile from human experiment (dashed) baseline trial (1m/s) and GRF from simulated gait (solid). GRF of unassisted-leg (red) and assisted leg (black) are normalized by body weight.	43
Figure 10:	a) An example of the range of tolerable gait deviations under the influence of Set-point controller (orange crosses) and of coordination controller (blue dots). The nominal joint angles are indicated by the black circle. b) Peak joint torque profile (color bar in Nm) needed to restore nominal gaits in cases of the coordination controller (top) and set-point controller (bottom). The torque signature spans across tolerable range of gait deviations of knee (x axis) and hip (y axis) of the assisted side.	45
Figure 11:	a) An example of evolutions of hip forward velocities over the assisted-leg swing (black) and unassisted-leg swing (red). The model driven by set-point controller (dots) and coordination controller (line) adapts to push-off impulse. b) The cadence of the unassisted sides (red) and assisted sides (black) driven by coordination controller (line) and set-point controller (dots) in response to push-off impulse.	46
Figure 12:	Hip forward velocity of the model in response to push-off impulse applied at the unassisted side liftoff (UL). The terminal speed of model driven by Coordination Strategy (blue) and Set-point Control (orange)	47
Figure 13:	a) Average step frequency over 50 steps due to varying intensities of push-offs under different control strategies. b) Final step lengths in relation to the magnitude of push-off impulse under influence of different controllers.	47

Figure 14:	The geometric coupling between the assisted hip joint angles and gait progression of unassisted side indicated by are shown. Assisted hip angles of walking at numerous speeds are plotted against during the unassisted single stance.....	49
Figure 15:	a) Changes in hip forward velocity due to push-off impulses (normalized by body weight) driven by interlimb coordination (blue) and set-point control (orange). b) Changes in walking speeds in response to changes in effective push-off impulses (normalized by body weight) over propulsive phase.....	49
Figure 16:	Active-leg Exoskeleton (ALEX) robotic platform for post-stroke gait-training.....	60

ABSTRACT

Bipedal locomotion is a routine and yet sophisticated task. Studies looking at biological systems suggest that bilateral coordination is the key to articulated rhythmic motions such as walking. Given its importance in formulating human walking, the potential of promoting *interlimb coordination* to facilitate gait-training for post-stroke patients who suffer impaired motor function due to neurological lesions, has NOT been fully explored. Current strategy primarily focused developing a more normal swing pattern on the affected side, but the results had mixed success so far. The gait-training community has yet to close the loop between prescribing the *appropriate* interventions and evaluating corresponding changes on either biomechanical or neurological domain.

Inspired by a series of reduced-order locomotion models, this thesis aims at proposing a model framework, or a “template”, that enables systematic evaluation of the effects of gait-training strategies on gait performance outcomes. This template can capture dominant features of bipedal locomotion without delving into the fine details of human anatomic structure and morphology. Key metrics of human walking gaits including the evolution of center of mass, joint patterns, ground reaction force etc. was demonstrated. Additionally, the template allows custom control schemes and characterization of joint torques for swing motion, driven by interlimb coordination in particular. This enables differentiating the performance of coordination strategy against the incumbent in gait stability, energetic efficiency, and response to speed modulations.

Through careful analysis of the model simulations and comparable experimental data, this proposed model not only proved its value in unifying the design and evaluation of gait-training strategies, also provided insights into the potency of a coordination-centric approach as a gait-training strategy.

Chapter 1

INTRODUCTION

1.1 Bilateral Coordination

Bipedal locomotion is a routine and yet sophisticated task, achieved by a series of coordinated body segments performing collaborative and competitive tasks (i.e. balance, body support and forward progression) [1]. Studies looking at biological systems from an evolution perspective suggest that bilateral coordination is rooted in the locomotion of quadrupedal [2]–[4] and bipedal [5]–[7] animals, and is a primary building block to formulating articulated rhythmic motions such as walking and cycling [8]. Interlimb coordination, which refers to the timing of motor cycles in limbs related to the contralateral counterparts [9], has been supported by evidence from both neuro-physiological [10] and biomechanical domains [11].

As one of the leading causes for long-term disability in older adults [12], *stroke* affects approximately 795,000 people in the United States each year. Neurological impairment caused by stroke can lead to impaired interlimb coordination as a consequence of lesions in specific supraspinal neuronal structures, resulting in asymmetric lower limb motor impairment [13]–[15]. Due to impaired motor function, stroke survivors usually suffer from residual gait deficits [16]–[21] and substantial limitations in functional ambulation [22], [23].

Gait-training that involves repetitive practice of the affected limb has been central to enhancing impaired motor functions for post-stroke individuals. The paretic side alone is facilitated by external assistance, applied by either therapists or robotic

technology, to develop a more normal swing pattern. Short-term learning of a novel trajectory in healthy individuals has been shown with robotic training using error feedback [24], [25] and recently extended to stroke survivors [26]. However, the efficacy of the current strategy that engages the paretic side in following exogenous walking templates has had mixed success in restoring gait aesthetics and functional ambulation [27]–[30].

Given the importance of interlimb coordination to formulating human walking gaits, the potential of promoting interlimb coordination to facilitate gait-training can be transformational to the existing rehabilitation landscape. Studies exploring the potency of interlimb coordination as the objective of gait-training have indicated promising results [31]–[33], and evidence has shown that novel interlimb coordination patterns can be trained and retained after split-belt treadmill training [34].

1.2 Reductive Model

Despite the enormous collection of work assessing the efficacy of gait-training, there is a lack of a basic modelling framework capable of providing guidelines to prescribing adequate assistance to the subject and evaluating the corresponding effects of prescribed interventions on gait characteristics and performance. As an attempt to close this loop, we propose a template model that not only captures the underlying dynamics of bipedal walking but also possesses the abilities to delineate the joint effort needed by the paretic limb. Existing musculoskeletal models [35], [36], which delve into the full details of muscular activation patterns, are able to capture gait kinematics and dynamics. However, they fail to capture the nominal cyclicity of human walking, which is very crucial for determining adequate assistive strategies in gait-training.

Reduced-order bipedal models however have been instrumental to reducing the complexity associated with modelling muscular activity, while preserving the central ingredients needed to produce a variety of bipedal gaits, in a unified fashion [37]. An important example of the reductive bipedal models is the double spring-loaded inverted pendulum (D-SLIP) model [38], [39]. The model captures key characteristics of walking gait like double stance and is successful in reproducing human-like gait features such as ground reaction force (GRF) and oscillatory movements of the center of mass (CoM). It provides the foundational analytic framework for studying the critical performance metrics (speed, step length, energetics and etc.) of a variety of bipedal gaits [40].

Despite of the success of the D-SLIP model in reproducing kinematics and kinetics of human walking with such a lean setup, it is clearly limited by its passive nature. For example, the D-SLIP model provides no means to characterize the effort required to cycle the limbs repeatedly during the swing phase, and hence is silent about devising appropriate interventions, which is critical for gait rehabilitation treatments. In addition, the post-stroke subjects bear substantial deficiencies in motor functions of the affected side, which are not captured by D-SLIP model. The affected limb usually suffers from a limited range of motion and weakened muscle activations, resulting in limited mechanical capability to perform functions such as push-off [41]. The current D-SLIP model is not prepared to account for such inherent mechanical and functional asymmetry in hemiparesis.

Therefore, we propose a template planar model that is a continuum of the early work [42]. Our model (Figure 1a) underscores the asymmetric nature of hemiparetic subjects by differentiating the affected and unaffected legs mechanically and functionally. The point mass M representing the upper body mass pivots about the leg

end which is in fixed contact with the ground. The unaffected/unassisted side is represented by a SLIP model, which has been shown to be very successful in modeling walking gaits of neurologically-intact subjects. Additional impulse is introduced at the unassisted limb push-off to simulate the effort to modulate walking speeds. This is primarily due to the dominant effect of ankle push-off to gait functions. The paretic/assisted side however, unlike the standard D-SLIP model which is symmetric, is represented by a two-link system augmented by actuations at the hip and knee joints, which enables quantitative characterization of control effort based on different training strategies.

The template model proposed provides the necessary ingredients for prescribing an interlimb coordination policy between the two sides, or any other training schemes

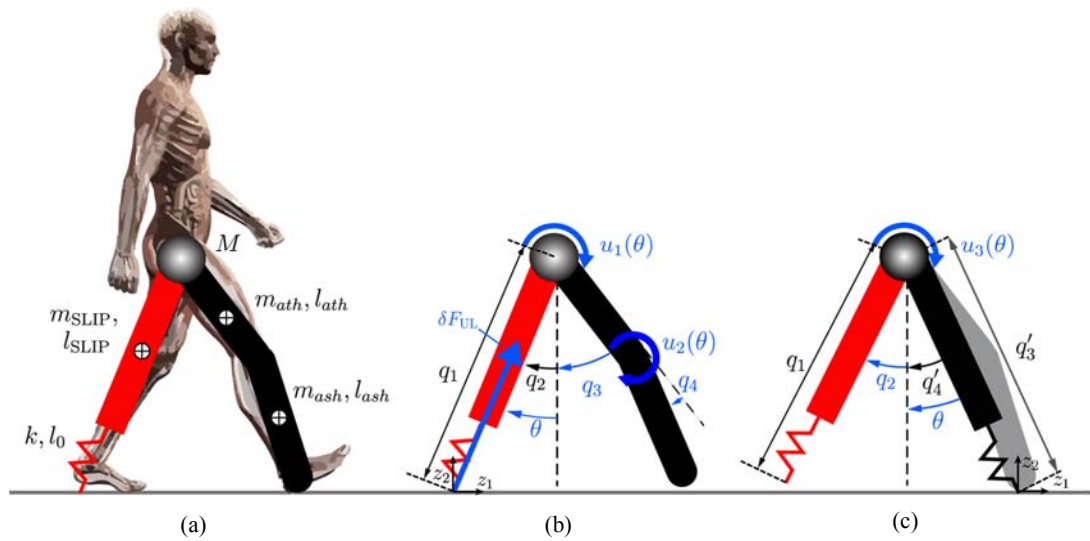


Figure 1: Reduced-order model of human locomotion. a) 4 degrees-of-freedom model with an asymmetric leg setup: the unassisted/affected side (red) and the two-link assisted/affected side (black); model parameters (mass, length) of each segment are shown. b) two-link assisted leg model with joint torque at assisted hip (u_1) and assisted knee joints (u_2) that are coupled with gait variable (θ) during assisted-leg swing phase; Push-off effort by the unassisted-leg side at its liftoff is modeled as an impulse (δF_{UL}) along the unassisted leg. c) D-SLIP model with unassisted hip torque (u_3) during unassisted-leg swing.

involving coordinated movements, which could have a far-reaching impact on developing and evaluating new gait-training paradigms. The coordination pattern will be formulated by characterizing the joint motions of the assisted joints (q_3, q_4) during swing phase according to gait progression of the contralateral side (θ) in Figure 1b, creating a bilateral kinematic coupling. This setup allows gait-training schemes to target at various aspects of gait (e.g. hip, knee, or combination of joints) by modifying the parameters pertaining to coordination patterns. This is of immense importance because the model provides quantifiable objectives for therapists in order to customize the training schemes and continuously challenge post-stroke individuals in gait-training.

With this modelling framework, we can close the loop between the design of interventions and assessment of therapeutic outcome, by adjusting the interlimb coordination patterns (training strategies) and evaluating the training outcome all in one picture. To validate that interlimb coordination can serve as a viable guideline for gait-training, we simulated the walking gaits based on interlimb coordination, compared the gait performance driven by bilateral policy against standard gait-training strategy in simulation, and validated the results with experimental data from healthy subjects walking on instrumented treadmill. In summary, the objective of this work is to:

- 1) introduce a model template which enables quantitative investigations of multiple control strategies and corresponding performance on post-stroke gait-training;
- 2) determine whether interlimb coordination is a feasible gait-training strategy by showing its capability to producing stable and robust walking gaits; and,
- 3) confirm that interlimb coordination is preserved at different speeds and it is a viable strategy for gait-training to modulate speed with human experiment validation

Chapter 2

MODEL

2.1 Reduced-order Biped Model

A reduced-order model is proposed in this work as the basic framework for the locomotion of the healthy and hemiparetic subjects (Figure 1). In contrast to D-SLIP model which has a symmetric setup, our model differentiates the unassisted (red) and the assisted (black) side with distinct leg models (Figure 1a). This provides finer resolution of the limb movement and joint torque profile needed to achieve desirable walking gaits. With the access to these richer details, it opens doors to investigating and customizing adequate joint efforts, individually or collaboratively for each subject of interest. This is instrumental to the design of gait training schemes as this setup now can afford the iterative process of searching for the appropriate joint actuations to facilitate the movements of the assisted side.

In order to delineate the joint efforts during different phases of the gait cycle, two sets of leg models are defined to capture the different locomotive functions of the assisted leg during its swing and stance respectively. When the assisted leg is in the air, it is represented as a two-link model with distinct hip and knee joint actuations (Figure 1b). On the other hand, during its stance, the assisted side adopts the same SLIP model as its unassisted counterpart, and hence the model takes the form of a D-SLIP model with leg mass (Figure 1c).

The sequence of phases in a gait cycle is shown in Figure 2. A gait cycle is consisted of alternating continuous phases indicated by arrows and discrete events indicated by triangles. Each continuous phase is terminated at an event where certain

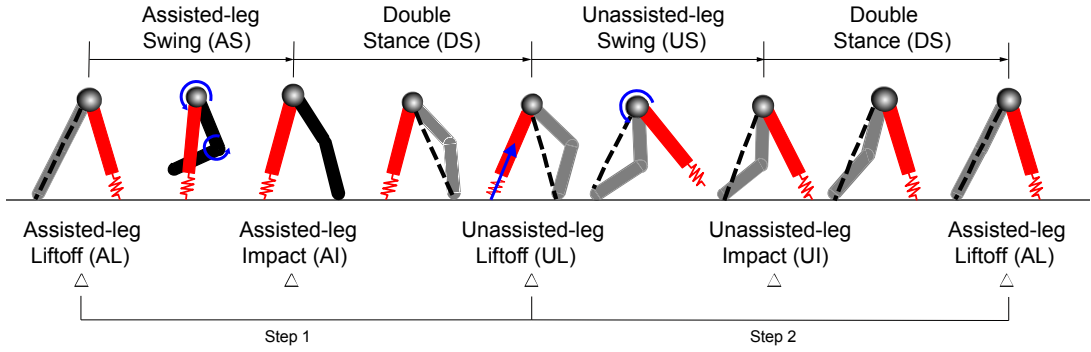


Figure 2: Continuous phases and transitional events of the gait cycle for the reduced-order biped model

terminal conditions are satisfied, and the model is ready for the next phase. There is a total of 4 continuous phases, each accompanied by its terminal event. For example, the model in Figure 2 starts with the assisted-leg swing (AS) phase, where the assisted leg takes off from the ground and moves forward with actuations at the hip and knee joints. The phase is terminated at an event when the assisted-leg impacts (AI) with ground. Each continuous phase and its terminal event, such as AS and AI, constitute a subsection of the gait cycle and the corresponding dynamics will be outlined in later sections. The model then enters the first double stance (DS) phase where both legs remain fixed contact with the ground. The DS phase ends at the unassisted leg liftoff (UL) when the unassisted leg is fully extended. This concludes the first step taken by assisted leg. The second step follows the same sequence of phases and events: unassisted-leg swing (US), unassisted-leg impact (UI), second double stance (DS) and eventually ends at assisted-leg liftoff (AL) where the cycle begins.

At the leg impacts (AI and UI), the leg-ground impact is modeled as inelastic impact and the detailed assumptions of the impact can be found in [43]. On the other hand, at liftoff events, the leg takes off when it is fully extended to its natural length l_0 . Because the model changes the assisted leg model depending on whether it is in the air

(Figure 1b) or in stance (Figure 1c), the model uses two sets of generalized coordinates: $q_{AS} = (q_1, q_2, q_3, q_4, z_1, z_2)^T$ and $q_i = (q_1, q_2, q'_3, q'_4, z_1, z_2)^T$ where $i \in \{DS, US, DS\}$. Cartesian coordinates z_1, z_2 are the ground contact point of the stance-leg, which remains at a fixed location during its stance. When the model switches its coordinates, the hip position remains unchanged relative to the leg-ground contact point (toe). The two-link model is replaced by a SLIP model that connects the hip joint and toe, and vice versa. A coordinate transformation $\gamma: q' = \gamma(q)$ can be performed to obtain the D-SLIP configuration q' from the original coordinate q . The length and mass of the assisted leg are preserved during the transition. This replacement can be visualized in Figure 2 as the dashed lines.

The model is constantly under the influence of active inputs during continuous phases and is affected by external impulses at the discrete events throughout the gait cycle. 3 joints of the model are actuated and they are only engaged during their respective swing phases shown in Figure 2: assisted hip (u_1) and knee (u_2) during AS phase, and unassisted hip (u_3) during US phase. No joint actuations are involved during DS phases. However, at the discrete events, the model is affected by external interactions whether with the ground at impacts or by active push-off effort at liftoffs. The effects of these interactions are directed to the model dynamics through impulses. For example, in an attempt to simulate the subjects' intention to modulate speed at the unassisted-leg liftoff, the effort to increase ankle push-off is abstracted as an impulse δF_{UL} along the unassisted leg (shown as a blue arrow in Figure 2).

A governing dynamics equation can be obtained by the Lagrange method for phase $i \in \{AS, DS, US, DS\}$,

$$\begin{aligned}
D_i(q_i)\ddot{q}_i + C_i(q_i, \dot{q}_i)\dot{q}_i + G_i(q_i) &= B_i u_i + J_i^T \lambda + E_i^T \delta F_i \\
\Phi_i(q_i) &= 0
\end{aligned} \tag{1}$$

where D_i , C_i , G_i are the inertia matrix, Coriolis matrix, and gravitational term respectively. Joint actuations u_i are mapped into the coordinate system by B_i . Lagrange multiplier λ that enforces the phase-based holonomic constraints $\Phi_i(q_i)$ is a set of holonomic constraints affects the dynamics via the Jacobian matrix $J_i = \frac{\partial \Phi_i}{\partial q_i}$. External impulses δF_i applied to the model at discrete events such as impacts and liftoffs affects the dynamics via the Jacobean matrix E_i . Selecting the state vector x to include the configuration variables and the corresponding rates, that is $x_i = (q_i^T, \dot{q}_i^T)^T$. Considering the assumptions (no impulse), the state-space form of the dynamics (1) can be expressed as a differential equation,

$$\begin{aligned}
\dot{x}_i &= \begin{bmatrix} \dot{q}_i \\ D_i^{-1} \left(-C_i \dot{q}_i - G_i + \left(\frac{\partial \Phi_i}{\partial q_i} \right)^T \lambda \right) \end{bmatrix} + \begin{bmatrix} 0 \\ D_i^{-1} B_i \end{bmatrix} u_i \\
&= f_i(x_i) + g_i(x_i)
\end{aligned} \tag{2}$$

During each continuous phase, the *continuous dynamics* (f_i, g_i) is a variation of equation (2) on a domain \mathcal{X} . The model continues evolving until it reaches the terminal events (leg impact or liftoff), which are described by threshold function $H_i(x_i) = 0$. This defines a *switching surface* S_i on which the model undergoes the discrete change of states that includes changes in the velocity of the system due to ground impacts or push-off effort, as well as change of coordinates due to model transformation. The end result is a *reset map* $\Delta_{i \rightarrow j}$,

$$x_j^+ = \Delta_{i \rightarrow j}(x_i^-) \quad (3)$$

mapping the pre-event states, x_i^- , to the post-event states, x_j^+ for the successive phase j . More details on deriving the reset map $\Delta_{i \rightarrow j}$ can be found in the book [43]. In the following sections, we will outline the common elements for each phase: the continuous dynamics, the switching surface and the reset map and present the dynamics for each pair of continuous phase and the terminal event.

2.1.1 Assisted-Leg Swing (AS) and Assisted-leg Impact (AI)

During the assisted-leg swing, the body mass pivots about the fixed unassisted-leg toe as the assisted leg swings forward. This gives rise to the phase-specific constraints $\Phi_{AS}(q): [z_1 - c_1, z_2 - c_2]^T = 0$ where c_1 and c_2 are constants. Since the unassisted-leg toe (z_1, z_2) remains at a fixed position, $\lambda \frac{\partial \Phi_{AS}(q)}{\partial q} = 0$ will render $\lambda \equiv 0$. The dynamics is subject to only control actions by hip and knee actuators. Therefore, $u_{AS} = (u_1, u_2, 0)^T$. Substituting the phase-specific quantities as outlined above in equation (1) yielding,

$$\begin{aligned} D_{AS}(q_{AS})\ddot{q}_{AS} + C_{AS}(q_{AS}, \dot{q}_{AS})\dot{q}_{AS} + G_{AS}(q_{AS}) &= B_{AS}u_{AS} \\ \Phi_{AS}(q_{AS}) &= 0 \end{aligned} \quad (4)$$

The model is written in state-space form by defining

$$\begin{aligned} \dot{x}_{AS} &= \begin{bmatrix} \dot{q}_{AS} \\ D_{AS}^{-1}[-C_{AS}(q_{AS}, \dot{q}_{AS})\dot{q}_{AS} - G_{AS}(q_{AS})] \end{bmatrix} + \begin{bmatrix} 0 \\ D_{AS}^{-1}B_{AS} \end{bmatrix} u_{AS} \\ &= f_{AS}(x_{AS}) + g_{AS}(x_{AS})u_{AS} \end{aligned} \quad (5)$$

The continues dynamics of the AS phase evolves until the vertical distance from the assisted-side foot to the ground becomes zero, captured by,

$$H_{AI}(q) := q_1 \cos(q_2) - l_{ath} \cos(q_2 + q_3) - l_{ash} \cos(q_2 + q_3 + q_4) \quad (6)$$

which defines the switching surface S_{AI} ,

$$S_{AI} := \{x | H_{AI}(q) = 0, \dot{H}_{AI}(q) < 0\} \quad (7)$$

The impact dynamics is a continuum of the continuous phase, and hence the constraints $\Phi_{AS}(q)$ of assisted-leg swing (AS) phase are still valid during the assisted-leg impact event. Now the model dynamics is affected by external impulses δF_{AI} due to the impact. Therefore, the dynamics can be expressed as,

$$\begin{aligned} D_{AS}(q_{AS})\ddot{q}_{AS} + C_{AS}(q_{AS}, \dot{q}_{AS})\dot{q}_{AS} + G_{AS}(q_{AS}) &= B_{AS}u_{AS} + E^T \delta F_{AI} \\ \Phi_{AS}(q_{AS}) &= 0 \end{aligned} \quad (8)$$

We model the impact as an inelastic collision [44], i.e. the leg impacts with the ground and does not slip or bounce. Both legs will remain in contact with the ground after impact. Thus, the configuration variables q are invariant after the impact. Following the Impact Hypotheses in [45], both sides of impact dynamics (8) can be “integrated” over the “duration” of impact, resulting in,

$$D_{AS}(q_{AS}^+)\dot{q}_{AS}^+ - D_{AS}(q_{AS}^-)\dot{q}_{AS}^- = E_{AS}^T F_{AI} \quad (9)$$

where $F_{AI} := \int_{t^-}^{t^+} \delta F_{AI}$ is the resultant impulsive force during the impact, and \dot{q}^- and \dot{q}^+ denote the pre- and post-impact velocity. The post-impact states satisfy

$$E_{AS}(q_{AS})\dot{q}_{AS}^+ = 0 \quad (10)$$

Combining (9) and (10), we obtain

$$\begin{bmatrix} D_{AS}(q_{AS}) & -E_{AS}^T(q_{AS}) \\ E_{AS}(q_{AS}) & 0_{4 \times 4} \end{bmatrix} \begin{bmatrix} \dot{q}_{AS}^+ \\ F_{AI} \end{bmatrix} = \begin{bmatrix} D_{AS}(q_{AS}^-) \dot{q}_{AS}^- \\ 0 \end{bmatrix} \quad (11)$$

The augmented matrix on the LHS of the above equation is invertible and the solution of equation (11) is unique and this results in,

$$\dot{q}_{AS}^+ = \Pi_{11}(q_{AS}^-) D_{AS}(q_{AS}^-) \dot{q}_{AS}^- =: \Delta_q \dot{q}_{AS}^- \quad (12)$$

where

$$\Pi(q_{AS}) = \begin{bmatrix} D_{AS}(q_{AS}) & -E_{AS}^T(q_{AS}) \\ E_{AS}(q_{AS}) & 0_{4 \times 4} \end{bmatrix}^{-1} \quad (13)$$

Π_{11} is the a 6-by-6 block matrix composed of the first 6 rows and first 6 columns of the matrix Π_{11} .

After the impact, the model switches to a D-SLIP setup. Therefore, a state transformation Γ is necessary to obtain the post-impact states that will be ready for the next phase. Combining with (12), the assisted-leg impact dynamics shown in (8) can be expressed as a mapping from the pre-impact states x_{AS}^- to post-impact states x_{DS1}^+ ,

$$x_{DS}^+ = \Delta_{AI}(x_{AS}^-) \quad x_{AS} \in S_{AI} \quad (14)$$

Δ_{AI} is the reset map for assisted-leg impact (AI).

2.1.2 Double Stance (DS) and Unassisted-leg Liftoff (UL)

After the assisted-leg impacts with the ground, the model enters the double stance phase where the location of the ground contact points (toes) on both sides are fixed with the

ground and the distance between the toes (step length) remains constant d . The resulting holonomic constraints become,

$$\Phi_{DS}(q_{DS}) := \begin{bmatrix} z_1 + q_1 \sin(q_2) + q'_3 \sin(-q'_4) - d \\ z_2 + q_1 \cos(q_2) - q'_3 \sin(-q'_4) \\ \Phi_{AS} \end{bmatrix} \quad (15)$$

where Φ_{AS} is the constraints during the AS phase. During the double stance phase, no voluntary control effort or external impulse is engaged, and hence $u_{DS} = 0$ and $\delta F_{DS} = 0$, which result in dynamic equation for DS phase,

$$\begin{aligned} D_{DS}(q_{DS})\ddot{q}_{DS} + C_{DS}(q_{DS}, \dot{q}_{DS})\dot{q}_{DS} + G_{DS}(q_{DS}) &= \lambda J^T \\ \Phi_{DS}(q_{DS}) &= 0 \end{aligned} \quad (16)$$

In order to bring this to the state-space form, we will eliminate λ by differentiating (15) with respect to t twice,

$$\dot{J}\dot{q}_{DS} + J\ddot{q}_{DS} = 0 \quad (17)$$

and solve for Lagrange multiplier λ in (16) using (17), to get

$$\lambda = (JD^{-1}J^T)^{-1}[-\dot{J}\dot{q}_{DS} + JD^{-1}(C\dot{q}_{DS} + G)] \quad (18)$$

Finally, (16) can be written in state-space form as,

$$\begin{aligned} \dot{x}_{DS} &= f_{DS}(x_{DS}) \\ &= \begin{bmatrix} \dot{q}_{DS} \\ D^{-1}(q_{DS})[\lambda J^T - C(q_{DS}, \dot{q}_{DS})\dot{q}_{DS} - G(q_{DS})] \end{bmatrix} \end{aligned} \quad (19)$$

The double stance phase terminates when the unassisted leg is fully extended to its natural length l_0 , which can be described by another threshold function,

$$H_{UL} := q_1 - l_0 \quad (20)$$

which defines the switching surface S_{UL} ,

$$S_{UL} := \{x_{DS} | H_{UL}(q_{DS}) = 0, \dot{H}_{UL}(q_{DS}) > 0\} \quad (21)$$

The discrete dynamics during UL is affected by the push-off impulse applied at the toe of unassisted side towards the body mass, denoted as δF_{UL} . This gives rise to the dynamics for the unassisted-leg liftoff phase with push-off impulse,

$$\begin{aligned} D_{DS}(q_{DS})\ddot{q}_{DS} + C_{DS}(q_{DS}, \dot{q}_{DS})\dot{q}_{DS} + G_{DS}(q_{DS}) &= \lambda J^T + \delta F_{UL} \\ \Phi_{DS}(q_{DS}) &= 0 \end{aligned} \quad (22)$$

in which the holonomic constraints Φ_{DS} for double stance are still valid during unassisted-leg liftoff. The impulse δF_{UL} is not included in system dynamics during the nominal walking gait, but only appears when the subject intends to undergo speed modulation. Like transition at Assisted-Leg Impact (AI), the effect of dynamics during Unassisted-Leg Liftoff (22) can be represented as a mapping between pre- and post-liftoff states. The derivation procedure can follow (9)-(14) and the details are omitted. The final result is,

$$x_{US}^+ = \Delta_{UL}(x_{DS}^-) \quad x_{DS} \in S_{UL} \quad (23)$$

This completes the first step taken by the assisted leg. The second step (from US to AL) presents the same sequence of continuous phases and discrete events, except that

the unassisted side swings forward and there is no push-off effort at Assisted-leg Liftoff (AL).

2.1.3 Unassisted-leg Swing (US) and Unassisted-leg Impact (UI)

During the unassisted-leg swing (US), the model is unilaterally actuated by the joint torque at the unassisted hip, giving rise to a joint input $u_{US} = (0, 0, u_3)^T$. Like the assisted-leg swing, the model is only constrained at toe on the assisted side which is in stance now. This results in $\Phi_{US} := [z_1 - c_1, z_2 - c_2]^T = 0$. Therefore, the model has a continuous dynamics in the similar form of (4),

$$\begin{aligned} D_{US}(q_{US})\ddot{q}_{US} + C_{US}(q_{US}, \dot{q}_{US})\dot{q}_{US} + G_{US}(q_{DS}) &= B_{US}u_{US} + J^T \lambda \\ \Phi_{US}(q_{US}) &= 0 \end{aligned} \quad (24)$$

which can be written in state-space expression,

$$\dot{x}_{US} = f_{US}(x_{US}) + g_{US}(x_{US})u_{US} \quad (25)$$

The switching surface S_{UI} for unassisted-leg swing is defined at the event of unassisted-leg impact (UI), where the vertical distance between the unassisted-leg toe and ground, monitored by the threshold function H_{UI} , reduces to zero when the unassisted leg is in front of the hip. Thus, the switching surface S_{UI} can be defined,

$$S_{UI} := \{x \in \mathcal{X}_{US}, q'_3 > 0 | H_{UI}(q) = 0, \dot{H}_{UI} < 0\} \quad (26)$$

Similar to (14), the effect of this impact can also be expressed as a reset map between post- and pre-impact states,

$$x_{DS}^+ = \Delta_{UI}(x_{US}^-) \quad x_{US} \in S_{UI} \quad (27)$$

2.1.4 Double Stance (DS) and Assisted-leg Liftoff (AL)

Now the model enters the second double stance (DS) phase. Compared to the first, the unassisted and assisted sides swap positions. Similarly, the model is not subject to any joint inputs $u_{DS} = 0$ and both toes are subject to the same constraints as DS. Hence the dynamics of this DS phase can be expressed as,

$$\dot{x}_{DS} = f_{DS}(x_{DS}) \quad (28)$$

The dynamics of double stance follows (19), until the trailing assisted SLIP leg reaches its natural length l_0 , which is captured threshold function $H_{AL} = q'_3 - l_0$. Hence the switching surface S_{AL} can be defined by,

$$S_{AL} := \{x_{DS} | H_{AL}(q_{DS}) = 0, \dot{H}_{AL}(q_{DS}) > 0\} \quad (29)$$

A mapping Δ_{AL} between the pre-liftoff states and post-liftoff states can be obtained as a result of the discrete dynamics for the assisted-leg liftoff. The inverse state transformation Γ^{-1} is applied to the post-liftoff states x_{DS}^+ to re-initiate the model states in the original coordinates q_{AS} for the coming gait cycle. The reset map takes the pre-liftoff states to post-liftoff states in the original coordinates q_{AS} ,

$$x_{AS}^+ = \Delta_{AL}(x_{DS}^-) \quad x_{DS} \in S_{AL} \quad (30)$$

2.1.5 Summary of Model Dynamics

In summary, the full cycle consisting of 4 continuous phases accompanied with 4 distinct transitions can be expressed as a set of 4 non-linear subsystem with impulse effects as below,

$$\begin{aligned}
\Sigma_1: & \begin{cases} \dot{x}_{AS} = f_{AS}(x_{AS}) + g_{AS}(x_{AS})u_{AS} \\ x_{DS}^+ = \Delta_{AI}(x_{AS}^-) \end{cases} & x_{AS} \in S_{AI} \\
\Sigma_2: & \begin{cases} \dot{x}_{DS} = f_{DS}(x_{DS}^-) \\ x_{US}^+ = \Delta_{UL}(x_{DS}^-) \end{cases} & x_{DS} \in S_{UL} \\
\Sigma_3: & \begin{cases} \dot{x}_{US} = f_{US}(x_{US}) + g_{US}(x_{US})u_{US} \\ x_{DS}^+ = \Delta_{UI}(x_{US}^-) \end{cases} & x_{US} \in S_{UI} \\
\Sigma_4: & \begin{cases} \dot{x}_{DS} = f_{DS}(x_{DS}^-) \\ x_{AS}^+ = \Delta_{AL}(x_{DS}^-) \end{cases} & x_{DS} \in S_{AL}
\end{aligned} \tag{31}$$

Each of the 4 sub-systems is a *system with impulse effects*, a dynamical system that exhibits both continuous and discrete dynamic behavior. The presence of impacts and the varying nature of the contact conditions of the leg ends with the environment throughout a walking cycle -- due to leg touchdown and lift-off -- necessarily lead to a model that has multiple phases, and hence is hybrid.

2.2 Periodic Gait Cycle and Poincaré Return Map

This section develops the methods for determining the existence and stability properties of periodic orbits in nonlinear systems with impulse effects in the context of human locomotion. These methods analyze the periodic orbits and their properties in a systematic way and make the computations of such periodic gaits more practical. Here we: 1) define periodic orbits of hybrid systems and their stability properties; and 2) introduce the Poincaré method for studying the existence and stability properties of the periodic solutions.

2.2.1 Periodic Solutions and Periodic Gait

An autonomous system with impulse effects consists of three components: an autonomous ordinary differential equation, $\dot{x}(t) = f(x(t))$, defined on some state space \mathcal{X} ; a hyper surface S at which the solutions of the differential equation undergo a discrete transition that is modelled as an instantaneous reinitialization of the differential equation; and a rule $\Delta: S \rightarrow \mathcal{X}$ that specifies the new initial condition as a function of the point at which the solution crosses S . The surface S is called *switching surface* and Δ the *reset map* [43].

$$\Sigma: \begin{cases} \dot{x}(t) = f(x(t)) & x^- \notin S \\ x^+(t) = \Delta(x^-(t)) & x^-(t) \in S \end{cases} \quad (32)$$

The sub-systems $\Sigma_1, \Sigma_2, \Sigma_3, \Sigma_4$ in (31) are all systems with impulse effects. The solution of the overall system can be defined by concatenating the solutions of each individual system in (31) according to the succession of Figure 2. A formal definition of solutions to a hybrid system can be found in [43].

We will be interested in periodic solutions. A solution $\varphi(t): [t_0, \infty) \rightarrow \mathcal{X}$ of the autonomous system with impact effects like (31) is *periodic* if there exists a finite $T > 0$ such that $\varphi(t + T) = \varphi(t)$ for all $t \in [t_0, \infty)$, i.e. if the model is initiated at time t_0 , its states including joint angles and velocities at any instance, are identical to the states at time T later. A set $\mathcal{O} \subset \mathcal{X}$ is a *periodic orbit* of (31) if $\mathcal{O} = \{\varphi(t) \mid t \geq t_0\}$ for some period solution $\varphi(t)$. Human walking gaits are nontrivial periodic orbits of the dynamical system derived in section 2.1. A periodic orbit \mathcal{O} is *transversal* to the switching surface S if its closure intersects S at exactly one point, and at the intersection, the periodic orbit is not tangent to S (Figure 3).

A periodic orbit \mathcal{O} is *stable in the sense of Lyapunov* if for every $\epsilon > 0$, there exists an open neighborhood \mathcal{V} of \mathcal{O} such that for every $p \in \mathcal{V}$, there exists a solution $\varphi(t): [0, \infty) \rightarrow \mathcal{X}$ satisfying $\varphi(0) = p$, $\text{dist}(\varphi(t), \mathcal{O}) < \epsilon$ for all $t \geq 0$, where $\text{dist}(p_1, p_2)$ is the usual Euclidean distance between points $p_1, p_2 \in \mathbb{R}^n$ and $\text{dist}(p_1, \mathcal{O}) := \inf_{p_2 \in \mathcal{O}} \text{dist}(p_1, p_2)$. The orbit \mathcal{O} is *attractive* if there exists an open neighborhood \mathcal{V} of \mathcal{O} such that for every $p \in \mathcal{V}$, the solution $\varphi(t): [0, \infty) \rightarrow \mathcal{X}$ with $\varphi(0) = p$ satisfies $\lim_{t \rightarrow \infty} \text{dist}(\varphi(t), \mathcal{O}) = 0$. The orbit \mathcal{O} is *asymptotically stable in the sense of Lyapunov* if it is both stable and attractive. Finally, the orbit \mathcal{O} is *exponentially stable* if there exists an open neighborhood \mathcal{V} of \mathcal{O} and positive constants N and γ such that for every $p \in \mathcal{V}$, the a solution $\varphi: [0, \infty) \rightarrow \mathcal{X}$ with $\varphi(0) = p$ satisfies $\text{dist}(\varphi(t), \mathcal{O}) \leq N \text{exp}(-\gamma t) \text{dist}(p, \mathcal{O})$.

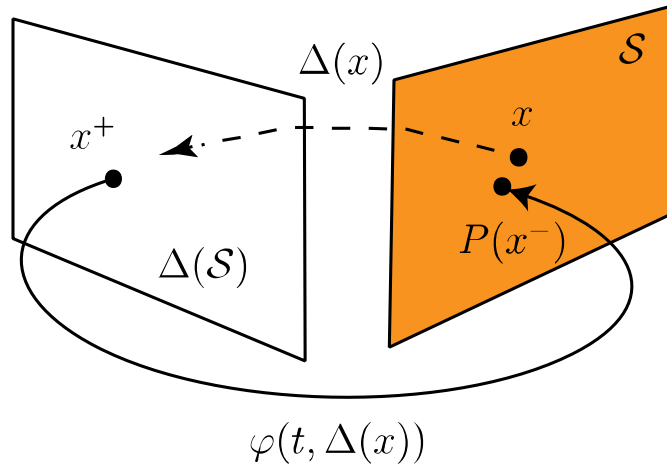


Figure 3: Geometric interpretation of a Poincaré return map $P: S \rightarrow S$ for a system with impulse effects. The switching surface S is selected to be the Poincaré section. The dashed line and solid line stand for the impact phase model and swing phase model, respectively. Δ is the impact map. $\varphi(t, \Delta(x))$ is a solution of the continuous phase.

2.2.2 Poincaré Return Map and Fixed Points

The dynamics of periodic walking gaits can be described by concatenating the dynamics of sub-systems in (31). To study the existence of such gaits, the method of Poincaré [46] is used. The Poincaré method examines the states of the model at a defined surface transversal to a periodic orbit, and studies the states of the discrete instances at two consecutive crossings with the surface. The defined surface is called Poincaré surface. There are natural choices for the Poincaré section, such as switching surface S . Without loss of generality, we will use the switching surface S_{AL} as the example; Note through that, the same procedure can be applied to other choices of such surface.

We will start by defining *flow maps* for each phase of the walking gait in Figure 2. The composition of the individual flow maps gives the Poincaré map.

Given the dynamics of the model, we first define the time-to-impact function for the Assisted-leg Swing (AS) phase, $T_{I,AS}: \mathcal{X} \rightarrow R \cap \{\infty\}$,

$$T_{I,AS} := \begin{cases} \inf\{t \geq 0 \mid \varphi_1(t, x_0) \in S_{AI}\} & \text{if } \exists t \text{ s.t. } \varphi_1(t, x_0) \in S_{AI} \\ \infty & \text{otherwise} \end{cases} \quad (33)$$

where φ_1 is the solution of the continuous phase AS represented by Σ_1 . Following the derivation in chapter of 4.2 of [43], the AS flow map that maps the entry states in AL to exit states for this phase at AI, $P_{AS}: S_{AL} \rightarrow S_{AI}$,

$$P_{AS}(x_{DS2}) := \varphi_{AS} \left(T_{I,AS}(\Delta_{AL}(x_{DS2})), \Delta_{AL}(x_{DS2}) \right) \quad (34)$$

where Δ_{AL} is the reset map that re-initializes the states coming into AS phase.

Following a similar derivation, the flow map for the DS1 phase corresponding to Σ_2 of Equation (31) $P_2: S_{AI} \rightarrow S_{UL}$,

$$P_2(x_{AS}) := \varphi_{DS} \left(T_{I,DS1}(\Delta_{AI}(x_{AS})), \Delta_{AI}(x_{AS}) \right) \quad (35)$$

is well defined and continuous. Similarly, the flow map for US phase $P_3: S_{UL} \rightarrow S_{UI}$; and DS2 phase $P_4: S_{UI} \rightarrow S_{AL}$, can be deduced,

$$P_3(x_{DS1}) := \varphi_{US} \left(T_{I,US}(\Delta_{UL}(x_{DS1})), \Delta_{UL}(x_{DS1}) \right) \quad (36)$$

$$P_4(x_{US}) := \varphi_{DS} \left(T_{I,DS2}(\Delta_{UI}(x_{US})), \Delta_{UI}(x_{US}) \right) \quad (37)$$

The Poincaré return map $P: S_{AL} \rightarrow S_{AL}$ for Equation (31) is defined by composing the flow maps for each phase sequentially,

$$P := P_4 \circ P_3 \circ P_2 \circ P_1 \quad (38)$$

The Poincaré return map gives rise to a discrete-time system on the Poincaré surface, S_{AI} for example, by defining

$$x[k+1] = P(x[k]) \quad (39)$$

and nominal periodic walking gaits are captured by the equilibrium points of (39). Such points are called fixed points x^* ,

$$x^* = P(x^*) \tag{40}$$

The method of Poincaré reduces the problem of studying the existence and stability properties of a periodic solutions to (31) down to studying the existence and stability properties of the equilibrium point of (39).

Based on Theorem 4.1 and Corollary 4.1 in [43], exponential stability of the gait cycle can be characterized by evaluating whether eigenvalues of the linearized Poincaré map at the fixed point x^* have magnitude strictly less than one.

2.3 Walking Pattern Generation

Section 2.2 provided the groundwork for defining the periodic orbits, i.e. the periodic walking cycle in the proposed model and its properties, as well as the Poincaré’s method to evaluate and guarantee the stability of such walking gaits. In this section, we propose a systematic framework for constructing such stable walking gaits by carefully choosing the appropriate control strategy to actuate the individual joints collaboratively. For the purpose of this work, we dedicate our attention to a bilateral strategy driven by interlimb coordination, where the movement of the assisted side is closely coupled with the unassisted side. Ultimately, the goal is to demonstrate the design of a feedback controller that creates asymptotically (or exponentially) stable walking gaits. This section has two objectives: 1) to present a class of output functions that govern interlimb joint coordination and 2) to introduce a finite parametrization of these outputs in a form that will permit the shaping of coordination patterns by parameter optimization.

2.3.1 Interlimb Coordination Strategy

Despite their morphological differences during the swing phase, both the assisted and the unassisted leg are not engaged in any active joint actions during the double stance as the D-SLIP model. However, during their swing phase, the controlled joints, regardless of assisted or unassisted side, are geometrically coupled to gait progression of the contralateral side in stance (Figure 4). Such geometric coupling can be embedded in a set of outputs, which are later enforced by feedback control. Interlimb coupling can be achieved by driving these suitably-selected outputs to zero using input-output linearization. Therefore, the joint motions of the swing leg are orchestrated according to their contralateral side, providing interlimb coordination.

The output function y_i captures bilateral coordination by taking the difference between the controlled joints q_i^c , and the desired joint profile $h_i^d(\theta)$ prescribed by the phase variable θ_i , which is a monotonic geometric variable describing the gait progression. To spell out the output function,

$$y_i := h_i(q_i, \theta_i) = q_i^c - h_i^d(\theta_i) \quad (41)$$

where $i \in \{AS, US\}$ and q_i^c specifies controlled joints. In the proposed control framework, and θ has to be monotonic during the swing phase. Therefore, it follows,

$$q_i^c := H_0 q_i \quad (42)$$

$$\theta_i(q_i) := c_\theta q_i \quad (43)$$

note that in (41), $h_i^d(\theta)$ is a function of the configuration variables (not time), and there it can be interpreted as a virtual holonomic constraint. Bilateral coordinated movements

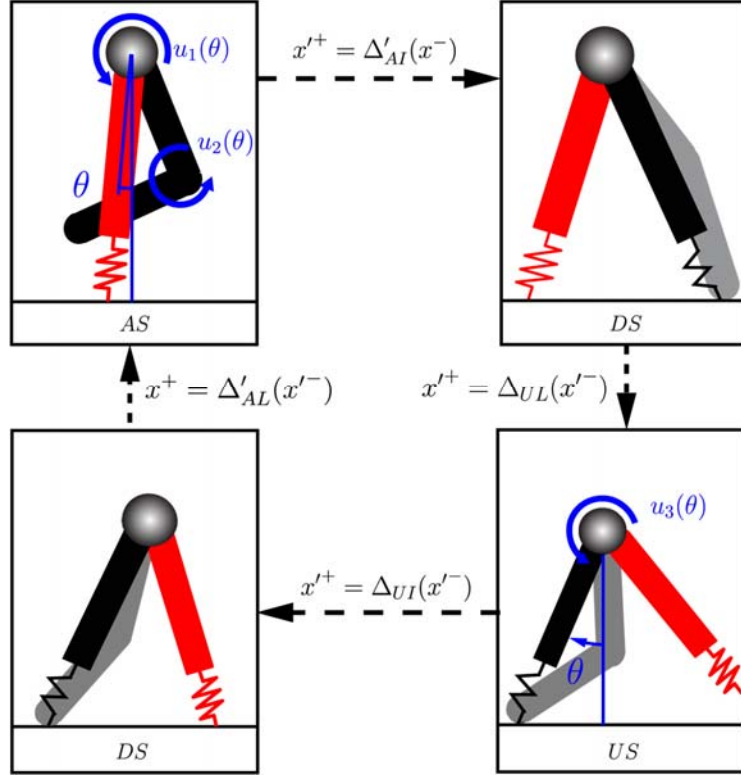


Figure 4: Evolution of the model during continuous phases and transition events and control schemes for each phase. The model is actuated during the swing phases (AS and US) by the joint torques (blue) that are coupled with gait progression variable θ . The model evolves along its intrinsic dynamics during the double stance phases.

are manifested in the formulation of the output function (41), as enforcing the joint motions of the swing side to follow joint profile that depends on the phase variable θ of the other side.

Taking the assisted-leg swing phase (AS) for example, the controlled variables q_c are the hip and knee joints of the assisted side, and the phase variable θ is the angle of the unassisted leg,

$$q_c = H_0 q = \begin{bmatrix} q_3 \\ q_4 \end{bmatrix} \quad (44)$$

$$\theta(q) = c_\theta q = q_2 \quad (45)$$

where $H_0 = \begin{bmatrix} 0 & 0 & 1 & 0 \\ 0 & 0 & 0 & 1 \end{bmatrix}$ and $c_\theta = [0 \ 1 \ 0 \ 0]$.

In order to realize the interlimb coordination patterns described in (41), the output function y has to be driven to zero by the torque available on the swing leg. The control actions required to promote the coordination strategy can be revealed by linearizing the input-output relationship along the swing phase dynamics.

From earlier derivations of (5) and (25), the dynamics of swing phase take a general form of: $\dot{x} = f(x) + g(x)u$. Through differentiation of output y , the control input u will be exposed and a linear relationship between inputs and outputs can be established. The first derivative of output along swing dynamics,

$$\frac{dy}{dt} = \frac{\partial h}{\partial x} \dot{x} \quad (46)$$

$$= \begin{bmatrix} \frac{\partial h}{\partial q} & \frac{\partial h}{\partial \dot{q}} \end{bmatrix} \left[\begin{bmatrix} \dot{q} \\ D^{-1}[-C\dot{q} - G] \end{bmatrix} + \begin{bmatrix} 0 \\ D^{-1}B \end{bmatrix} u \right] \quad (46a)$$

$$= \begin{bmatrix} \frac{\partial h}{\partial q} & 0 \end{bmatrix} \begin{bmatrix} \dot{q} \\ D^{-1}[-C\dot{q} - G] \end{bmatrix} + \begin{bmatrix} \frac{\partial h}{\partial q} & 0 \end{bmatrix} \begin{bmatrix} 0 \\ D^{-1}B \end{bmatrix} u \quad (46b)$$

$$= L_f h(q, \dot{q}) \quad (46c)$$

where $L_f h(q, \dot{q})$ denotes the Lie derivative of h along the vector field f . Since input u does not appear (46), differentiating the output once again computes the accelerations,

$$\begin{aligned}
\frac{d^2y}{dt^2} &= \left[\frac{\partial}{\partial q} \left(\frac{\partial h}{\partial \dot{q}} \right) \frac{\partial h}{\partial q} \right] \left[\left[D^{-1}[-C\dot{q} - G] \right] + \left[D^{-1}B \right] u \right] \\
&= \left[\frac{\partial}{\partial q} \left(\frac{\partial h}{\partial \dot{q}} \right) \frac{\partial h}{\partial q} \right] \left[D^{-1}[-C\dot{q} - G] \right] + \frac{\partial h}{\partial q} D^{-1}Bu \\
&= L_f^2 h(q, \dot{q}) + L_g L_f h(q)u
\end{aligned} \tag{47}$$

in which the matrix $L_g L_f h(q)$ is called the *decoupling matrix*, and it depends only on the configuration variables. The invertibility of this matrix at a given point ensures that u can influence the output function (47) and thus it ensures the existence and uniqueness of the desired control action. By driving $\ddot{y} = 0$ and assuming the decoupling matrix is invertible, the desired control effort u^* can be solved,

$$u^* = - \left(L_g L_f h(q) \right)^{-1} L_f^2(q, \dot{q}) \tag{48}$$

Despite the required torque to achieve coordinated joint movements and walking gaits, it is critical to ensure such gaits are attractive in the presence of external disturbances. In other words, the orbits must be asymptotically (or exponentially) stable. This can be achieved by deploying a feedback control that imposes the coordination patterns (41). As in,

$$u(x) = \left(L_g L_f h(x) \right)^{-1} \left(v - L_f^2 h(x) \right), \tag{49}$$

resulting in,

$$\frac{d^2y}{dt^2} = v \tag{50}$$

where v is chosen to according to the following PD control law

$$v = -\frac{1}{\epsilon} K_D \dot{y} - \frac{1}{\epsilon^2} K_P y \quad (51)$$

where $\epsilon > 0$ is a tuning parameter. Based on Theorem 5.5 detailed in section 5.5.2 in [43], the orbit \mathcal{O} is exponentially stable periodic orbit to (31) in closed loop with (49).

The same process can be replicated on the unassisted-leg swing (US) phase, where the unassisted hip joint is actuated, and the phase progression of the gait can be parametrized against the angle the assisted leg, which is now a SLIP model.

2.3.2 Desired Coordination Patterns

The desired joint profile $h_d(\theta)$ can be described by polynomial functions of θ , chosen to be the contralateral hip angle. Specifically, one-dimensional Bézier polynomials [45] of degree M are used to parameterize $h_d(\theta)$,

$$b_i(s) := \sum_{k=0}^M \alpha_k \frac{M!}{k!(M-k)!} s^k (1-s)^{M-k} \quad (52)$$

The Bézier polynomials of (52) have some useful features over others,

- a) The image of the Bézier polynomial is contained in the convex hull of the $M + 1$ coefficients
- b) $b(0) = \alpha_0$ and $b(1) = \alpha_M$
- c) $(\partial b_i(s)/\partial s) |_{s=0} = M(\alpha_1 - \alpha_0)$ and $(\partial b_i(s)/\partial s) |_{s=1} = M(\alpha_M - \alpha_{M-1})$

The first feature implied the polynomial does not fluctuate over small parameter variations, which is useful for numerical calculations. The next two features directly

relate coefficients α_0 and α_1 (α_{M-1}, α_M) to the starting (ending) configuration and velocity, which will significantly simplify the search for the desired coordination pattern.

A given gait phase variable $\theta(q)$ does not in general take values in the unit interval over a phase of single support. For appropriate construction of Bézier polynomials, the $\theta(q)$ will be normalized to fit the interval $[0, 1]$ as follows

$$s(q) := \frac{\theta(q) - \theta_s}{\theta_f - \theta_s} \quad (53)$$

where θ_s and θ_f are the values of θ at the starting and final states of single support phase.

Hence, the desired joint profile h_d parameterized by Bézier polynomials of the form (52) and (53) and it can be represented by $h_d \circ \theta(q)$,

$$h_d \circ \theta(q) := \begin{bmatrix} b_1 \circ s(q) \\ b_2 \circ s(q) \\ \vdots \\ b_{N-1} \circ s(q) \end{bmatrix} \quad (54)$$

We group the parameters α_k^i into an $(N - 1) \times (M + 1)$ matrix, α , and denote the columns of α by $\alpha_k := (\alpha_k^1; \dots; \alpha_k^{N-1})$. It is worthwhile to mention that the coordination patterns are determined by the polynomial coefficients α . As it is shown in the next section, they hold the key to constructing appropriate walking gaits of interests. Moreover, the optimization process provides tractable means to the design and customization of gait-training strategies to achieve the best therapeutic outcomes for individuals.

2.3.3 Gait Parameters Optimization

The previous two sections have specified a set of outputs for which the existence of the solutions to hybrid systems can be guaranteed in a straightforward manner. This section presents a general scheme for choosing the free parameters in Bézier polynomials to design a coordination strategy corresponding to α and the resulting walking gaits corresponding to a fixed point x^* . The main objective is to formulate the coordination strategy design problem as a parameter optimization problem. The optimization process will result in a feedback control law so that the corresponding closed-loop system which possesses an exponentially stable walking cycle. Along this solution a cost function will have been minimized while satisfying other kinematic and kinetic constraints.

The parameter selection problem will be cast as a constrained nonlinear optimization problem. The goal will be to choose the output function parameters α , such that hybrid model (31), the coordination strategy specified by (41) with q_i^d , q_i^c and θ_i as in (41), (42), (43), and state variable feedbacks given in (51), possesses an exponentially stable periodic orbit while minimizing a given cost function and satisfying a set of physically and mathematically motivated constraints along the periodic orbit.

The cost function chosen to be the energy expenditure by joints per distance traveled,

$$J(\alpha_j) := \frac{1}{\sum_j p_{swf,j}^h(q_j^-)} \int_0^{T_I} \sum_j \left(u_{\alpha_j}^*(t) \right)^2 dt \quad (55)$$

Where $j \in \{AS, US\}$, T_I is the cycle duration, $p_{swf,j}^h(q_j^-)$ corresponds to step length of each phase.

The optimization is subject to nonlinear constraints to ensure the feasibility of the walking gaits. Nonlinear inequality constraints (NIC) and nonlinear equality constraints (NEC) are chosen to ensure the following criteria are met:

NIC1) Minimal normal ground reaction force experience by stance leg,

NIC2) The vertical component of the post-impact trailing leg force is positive

NIC3) Anterior-posterior ground reaction forces are within the friction cone

NEC1) The existence of the fixed point

NEC2) The stability of the fixed point

NEC3) The average walking speed

The parameter optimization problem may be solved with any numerical optimization tools available. For this work, the optimization problem was solved with Matlab's (MathWorks, Natick, MA) `fmincon` solver with sequential quadratic program (sqp) algorithm.

2.4 Simulation Experiments

2.4.1 Set-point Control

Current gait-retraining strategies primarily focus on recovery of motor functions by engaging the paretic side in goal-oriented functional tasks such as these which practice intralimb coordination. The assistance particularly, by robotic gait-trainers, is administered based on how close the subject can follow certain time-position trajectories. In contrast to the bilateral strategy discussed previously, where the joint

motions on the paretic side are prescribed by the gait progress of the unassisted side, the patients are trained with playbacks of pre-fixed trajectories recorded from healthy subjects. One example of the training schemes uses the footpath recorded from of healthy subjects as the templates that the subjects are commanded to keep track of [24]. This approach is widely adopted by robotic gait-training platforms that target at gait rehabilitation for post-stroke subjects [47], [48].

This current control strategy can be mathematically formulated using inverse kinematics to map the footpath to the hip and knee joints. We will implement this control strategy in the proposed model framework and compare its performance with the interlimb coordination strategy. Similar to the interlimb coordination strategy, the alternative strategy can be formulated in the form of output functions (41), and the necessary joint control u_{alt} can be enforced by driving the output function to zero,

$$y'(t) := h'(q, t) = q_c - q'_d(t) \quad (56)$$

where $q'_d(t)$ is the time evolution of the configuration variables q . Following similar steps from (46)-(48), the joint torque profile required to maintain the prescribed trajectory can be obtained,

$$u_{alt}^*(t) = \left(L_f L_g h'(q, t) \right)^{-1} \left(-L_f^2 h'(q, t) + \ddot{q}'_d(t) \right) \quad (57)$$

However, in a practical gait-training session, following a prescribed trajectory can be problematic because a lag in time during trajectory tracking can lead to extraordinary torques that endanger the safety of subject [49]. Instead, the desired joint

position $q'_d(t)$, velocity $\dot{q}'_d(t)$ and acceleration $\ddot{q}'_d(t)$ during the swing phase of the simulated gait obtained by parameter optimization in Section 2.3.3, are discretized into point series respectively $Q_d[n] = (q_{d1}, q_{d2}, \dots, q_{dN})$, $V_d[n] = (\dot{q}_{d1}, \dot{q}_{d2}, \dots, \dot{q}_{dN})$ and $A_d[n] = (\ddot{q}_{d1}, \ddot{q}_{d2}, \dots, \ddot{q}_{dN})$. The discretized points can be stacked to form $S_d[n]$

$$S_d[n] = \begin{bmatrix} Q_d \\ V_d \\ A_d \end{bmatrix} = [S_d[1], S_d[2], \dots, S_d[N]] \quad (58)$$

where $S_d[n]$ is the i -th column vector of the discretized desired joint position, velocity and acceleration, and it is called the *set-point*.

At each iteration in the simulation, the objective of the controller is to bring the actual joint position to the geometrically closest set-point along the pre-specified trajectory where the Euclidean distance $|q_c(t) - q_d[n]|$ is the smallest. This set-point is denoted by S_d^* (Figure 5), i.e.

$$S_d^*[n] = \operatorname{argmin}_{q_d \in S_d, i \in N} |q_c(t) - q_d[i]| \quad (59)$$

consequently, the joint angle, velocity and acceleration of the set-point are denoted P_d^* , V_d^* , and A_d^* .

The output functions for set-point controller can be obtained by substituting the current set-point points into,

$$y_s := h_s(q) = q_c - Q_d^*[n] \quad (60)$$

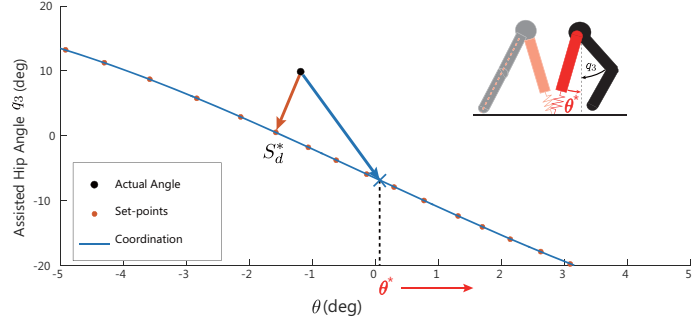


Figure 5: Schematics of the control objectives for the set-point controller and coordination controller

The nominal control law for set-point controller can be approximated by replacing the desired time evolution of joint motion in (57) with the set-point determined by (59),

$$u_s^* = \left(L_f L_g h_s(x) \right)^{-1} \left(A_d^* - L_f^2 h_s(x) \right) \quad (61)$$

where A_d^* is the acceleration of the desired set-point along the discretized path. Again, to ensure the nominal gaits are attractive, the PD control v in (51) is deployed with the exact same gains to ensure the converging behavior. Therefore, the control action applied by set-point control is,

$$u_s = \left(L_f L_g h_s(x) \right)^{-1} \left(v + A_d^* - L_f^2 h_s(x) \right) \quad (62)$$

2.4.2 Gait Stabilization

The capability of control strategies in restoring gait stability is the pillar to the design of gait-training paradigm. It is vital to investigate the performance of the control strategies in the cases where the subjects of interest develop abnormal gaits that deviate from desired joint patterns. Therefore, such scenarios are simulated in the model by starting the simulation at the instance of assisted-leg liftoff (AL), with hip and knee

angles on the assisted side slightly off the mark. We chose to introduce deviations at this instance because the control strategies would immediately respond to these disturbances and also has a longer time to respond to them before the assisted-leg touches the ground. Then we will evaluate whether the nominal gait can be recovered under the influence of control strategies with admissible control efforts. If the model can survive such gait deviation over 50 steps without failing, with the peak joint torque less than 100Nm, then the disturbance is claimed to be tolerable by the controller.

The joint angles on the assisted side will be disturbed by an increment of 5%, and the range of tolerable deviations can be obtained by recognizing the last largest deviation the model run on without failing. Simulations will be run on the full range of tolerable deviations in both cases of bilateral coordination and set-point control until the model fails the survival condition. The tolerable range of motion and the control efforts along both hip and knee joints will be compared.

2.4.3 Speed Modulation

Once control strategies demonstrate sufficient ability to stabilize walking gaits, we want to see whether they will respond to systematic gait changes, such as speed modulation.

The nominal walking gaits obtained from the parameter optimization will be simulated with interlimb coordination and set-point control strategies respectively. Speed modulation will be achieved by introducing additional repetitive impulse at unassisted-leg liftoff (UL) transition. The impulses are applied at the toe of the unassisted leg, directed along the leg pointing towards the hip. A variation of intensities of the impulses (normalized by body weight) are introduced in the simulation, all of which the model is ensured to survive the impulses and stabilize itself.

The forward speeds and step frequency over the AS and US phases are calculated for comparison. The evolutions of the hip speeds, step frequency and step length over time as well as their steady-state behaviors, will be evaluated across control strategies and impulse magnitudes.

Chapter 3

HUMAN EXPERIMENT

3.1 Research Design

Subjects are instructed to walk on a custom-built split-belt treadmill instrumented with two 6-component force platform (Bertec, Columbus, OH). The treadmill belt speeds are tied, and it can be set to two different modes: normal and user-driven. At normal mode, the treadmill is run at a fixed speed. At the user-driven mode, the belt speeds can adapt to the push-off forces (anterior GRF) applied to only one side, which is helpful for isolating the effect of the subject pushing off on one side. A diagram of treadmill control is shown in Figure 6.

The subjects will first be asked to identify their push-off side (left or right), which the treadmill control will be sensitive to. Demographic data including height, weight and age of the subjects will be recorded. Subjects will complete five trials: self-selected speed (Baseline) under normal mode, Pushoff-Adaptive (PA) speed under the user-driven mode and three fast speeds under normal mode: 20% faster (20Fast), 40% faster (40Fast), and 60% faster (60Fast) than baseline speed. During the Baseline trial, the magnitude of Anterior GRF (AGRF) are being recorded frame-by-frame. Upon the PA trial, 20 largest data points of AGRF will be averaged and the value will be displayed as visual reference in the next trial. During PA trial, given the visual reference, the subjects are encouraged to push harder against the treadmill than their Baseline trial on their push-off side to accelerate the walking speeds.

3.2 Participant

1 healthy subject (age 28 yrs., self-selected speed 1.0 m/s) is analyzed in this study.

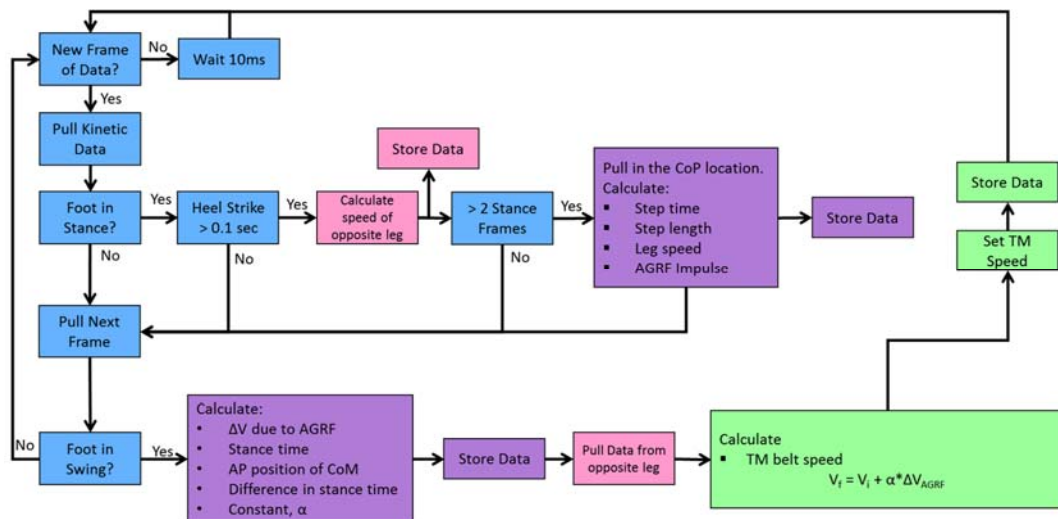


Figure 6: Control diagram of push-off adaptive treadmill control

3.3 Gait Evaluation

Kinematic and kinetic data are captured using an 8-camera (100Hz sampling rate) motion capture system (Motion Analysis Corp., Santa Rosa, CA, USA) as participants complete all trials a split-belt treadmill (Bertec, Columbus, OH) instrumented with 2 independent 6 degree of freedom force plate capturing at 2000Hz. Two rounds of these trials will be conducted to ensure repeatability. The self-selected walking speed is defined by slowly accelerating the treadmill until it reaches a speed that the participant claims that they are walking at their normal pace. Kinematic and kinetic data are filtered using a bi-directional Butterworth low-pass filter at 6 and 30 Hz, respectively.

3.4 Data Analysis

Kinematic and kinetic parameters in the sagittal plane including hip, knee angles and GRF are processed and averaged over the period of data collection for each trial. These results are used to compare with simulation results to validate the model.

The 2D acute angle formed between the line extension connecting the center of pressure (CoP) and the hip on the stance side and a vertical line are calculated, in order to monitor gait progression variable θ . The sign conventions follow the right-hand rule of the lab coordinates. The evolution of hip and knee joints of the non-dominant side at all speeds are matched with the progression of the contralateral side indicated by θ . Data processing is completed in Visual 3D (C-Motion Inc. Bethesda, MD).

We quantify push-off effort from subjects by calculating the area under the AGRF curve during the propulsive phase (Figure 7a). In order to make the measurements of push-off in experiment comparable to the one in simulations, *Effective Push-off Impulse* (I_{EPO}) is defined. It is the projection of the integral of AGRF over the period of propulsion phase onto the trailing limb angle at terminal configuration θ_f (Figure 7b).

$$I_{EPO} = \left(\int_{\text{Prop Phase}} \text{AGRF} \right) \sin(\theta_f) \quad (63)$$

The relationship between the walking speeds and effective push-off impulse are analyzed by using Pearson correlation coefficients to determine whether the impulse-speed relationship from the simulation can be validated by human subject data.

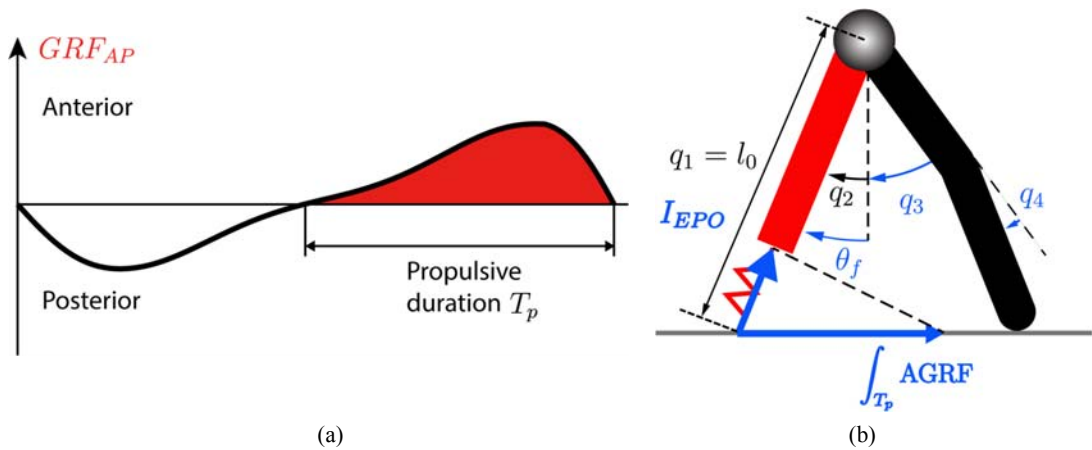


Figure 7: a) An illustration of the integral of anterior-posterior component of ground reaction force (GRF) profile during the propulsive duration T_p . b) an illustration of I_{EPO} as the projection of propulsive impulse along the unassisted-leg as the measurement of push-off impulse.

Chapter 4

RESULTS

4.1 Periodic Walking Gaits and Properties

A number of fixed points has been computed for different initial guesses and different coordination pattern coefficients using the model parameters in Table 1 and the optimization procedure discussed above. The model parameters listed refer to the work [38] and they are compliant to human anthropometric data in [50]. Figure 8(a)-(d) show an example of such fixed point by showing the evolution of the Cartesian variables of the hip joint during one gait cycle. As the hip joint is coincided with the body mass, it is demonstrated that the oscillation of the body mass reaches the peaks during both swing phases and re-bounces during the double stances (Figure 8a). The velocities of the body mass in both horizontal and vertical directions are damped due to the inelastic impact of the assisted leg with the ground, which results in a discontinuous drop in speed as shown in Figure 8(b) and Figure 8(d). The average hip forward speed over one cycle is 0.865 m/s.

Table 1: Model and Subject Parameters

Parameter	Model	Subject	Units
Body Mass (M)	64	56.2	kg
Assisted Thigh/Shank Mass (m_{ath}/m_{ash})	4	8.26/3.84	kg
Assisted Thigh/Shank Length (l_{ath}/l_{ash})	0.5/0.5	0.476/0.432	m
Assisted Thigh/Shank Inertia (J_{ath}/J_{ash})	0.083/0.083	0.143/0.061	kg m ²
Unassisted/SLIP Leg Mass (m_{SLIP})	8	12.1	kg m ²
Unassisted/SLIP Leg Inertia (J_{SLIP})	0.667	0.77	kg m ²
SLIP Leg Stiffness (k)	20	20.5	kN/m
SLIP Natural Length (l_0)	1.0	1.04	m

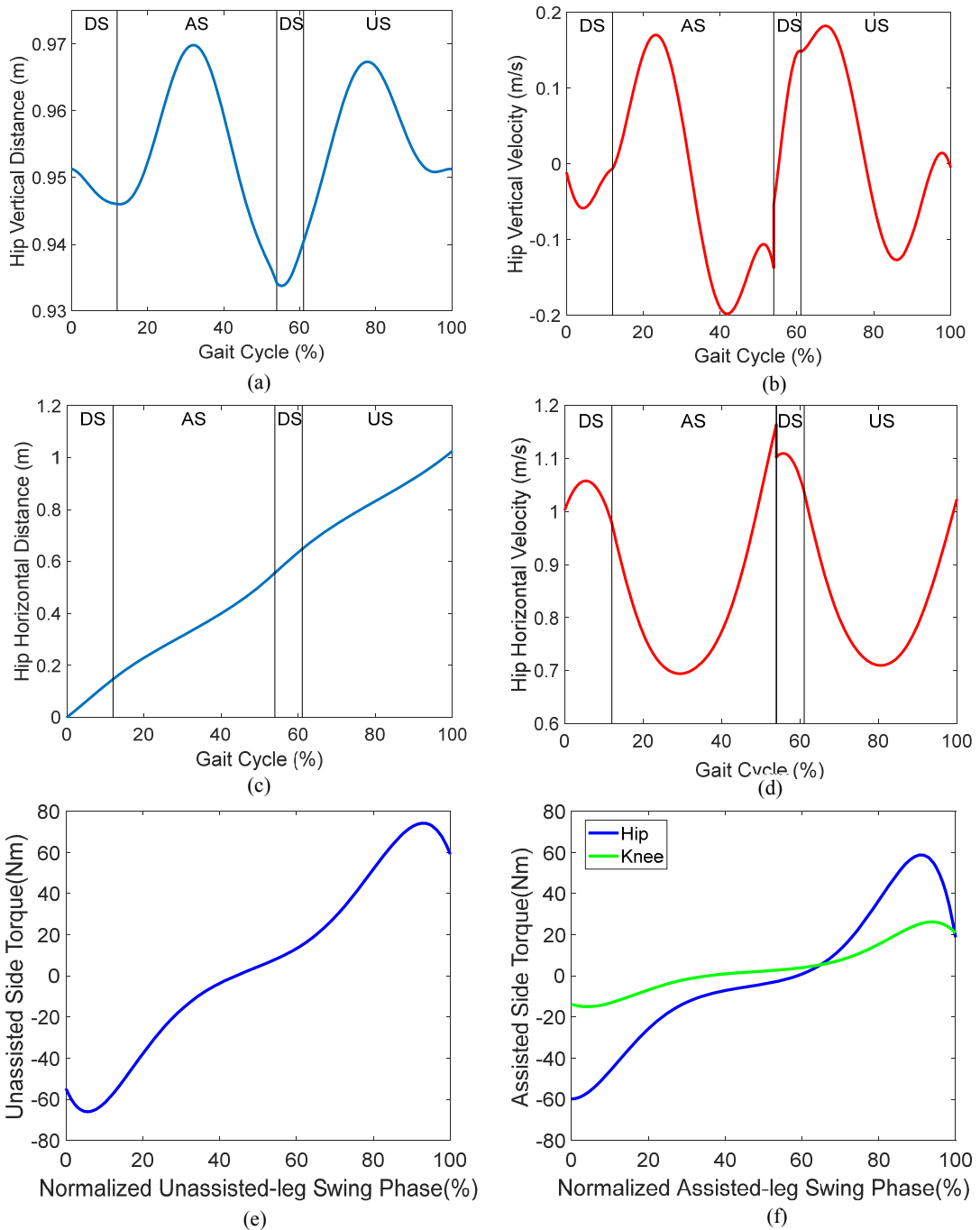


Figure 8: Evolution of the hip vertical displacement (a), hip vertical velocity (b), hip forward displacement (c) and hip forward velocity (d) during one gait cycle. The vertical lines correspond to the events; from left to right: assisted-leg liftoff, assisted-leg impact, unassisted-leg liftoff and unassisted-leg impact. The torque profile for unassisted side joint (e) and assisted side joints (f) during the normalized swing phase of the corresponding side. In (f), the blue and green line correspond to the hip and knee torques, respectively.

In addition, the joint torque profiles on both unassisted and assisted sides during their respective swing phase are demonstrated in Figure 8(e) and (f). Joints on both sides achieve the peak extension torques slightly before the leg impact. The values of the joint torques agree with observations of joint torques in human [51].

4.2 Model Validation

The evolution of hip and knee joints on the assisted side from the simulated gait over one cycle are demonstrated in Figure 9a respectively. The gait cycle starts from assisted-leg impact (AI) and ends with assisted-leg swing (AS) just before the impact. The evolution of gait cycle is normalized to be [0,100%]. The joint kinematics are displayed side-by-side with their counterparts from the baseline trial (1.0 m/s) of the human experiments (dashed line).

Our reductive model captures salient kinematic features of human walking. The range of motion for hip and knee joints shown in the model simulation are within the physically feasible range of human subjects and are comparable to the range shown in experimental data. The simulated gait shows late extensions on both hip and knee joints and late knee flexion compared to the joint evolutions from the experiment. Moreover, the simulated gait has a stance/swing duration ratio very close to the average 60%/40% split, which shows the model's ability to replicate human-like walking gaits.

In addition, the evolution of simulated ground reaction forces from both assisted and unassisted sides are displayed with the GRF profile from the experiments (Figure 9b). In the experimental data, the dominant side in stance is labelled as the "Unassisted Leg" (red) and the non-dominant side in stance as "Assisted Leg" (black). The simulated ground reaction forces (solid line) resembles to experimental data (dashed line). The anterior-posterior component (GRF_{AP}) of both sides from the simulated model follows

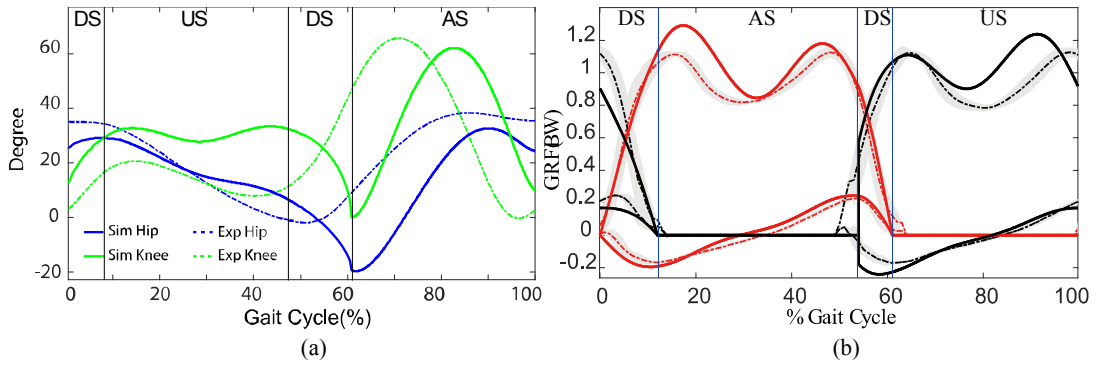


Figure 9: a) Joint kinematics of assisted-leg hip (blue) and knee (green) angle. The simulated joint angles (solid) and experimental joint outputs (dashed) are shown. The gait cycle starts at assisted leg impact and ends at assisted-leg swing just before impact, and the gait cycle is normalized. b) The mean and standard deviation of the GRF profile from human experiment (dashed) baseline trial (1m/s) and GRF from simulated gait (solid). GRF of unassisted-leg (red) and assisted leg (black) are normalized by body weight.

closely the profile of the experimental data. The vertical GRF profile in the model has shown the common double-hump shape on both sides, and it peaks at the same time during one gait cycle. Additional key gait kinematics from experiments are included in Table 2.

4.3 Potency of Interlimb Coordination for Gait-training in Simulations

4.3.1 Scenario I: Gait Stabilization

The model driven by (i) interlimb coordination strategy and (ii) set-point controller is each simulated at the fixed point found by parameter optimization and the performances of the model to withstand the gait deviations under the influence of different control policies are recorded in Figure 10a respectively. The coordination strategy shows a significant capability to recover from greater deviations from initial joint angles compared to its counterpart controller. The model driven by the coordination strategy sustains a range of gait deviations [-100%, +50%] of its initial hip

Table 2: Kinematic Parameters from Simulation and Experimental Results

Measurement	Model	Subject	Units
Speed	0.865	1.0	m/s
Ave Step Length	0.5	0.56±0.02	m
Ave Cadence	101.5	105.3±2.5	Steps/min
Stance/Swing Ratio	63%/37%	61%/39%	-
Peak Hip Angle	32.7	38.35	deg
Peak Knee Angle	62.2	65.8	deg
Speed	0.865	1.0	m/s
Ave Step Length	0.5	0.56±0.02	m

angle in simulation, and it recovered from deviations of up to 34 deg away from its initial knee angle. In contrast, the range of tolerable gait deviations along the hip angle is significantly limited to [-10%, 35%] when actuated by set-point controller, while it can handle up to 42 deg of knee angle deviations. The coordination strategy outperforms the set-point controller in restoring deviations at the hip and falls slightly behind on the tolerable range of motion at the knee joint.

The magnitude of peak joint torques to recover the nominal gait from the tolerable range of motion is color-coded in Figure 10b (top panel: interlimb coordination; bottom panel: set-point control). The set-point control, in general, requires more effort to recover the nominal gait for the same amount of gait deviations. In contrast, the effort by interlimb coordination strategy is comparatively smaller and it has a much smoother torque profile over the tolerable range of motion across both hip and knee angles.

4.3.2 Scenario II: Speed Modulation

The responses of the simulated walking gaits with respect to the effort to modulate walking speed via increasing push-off impulse depend on the control

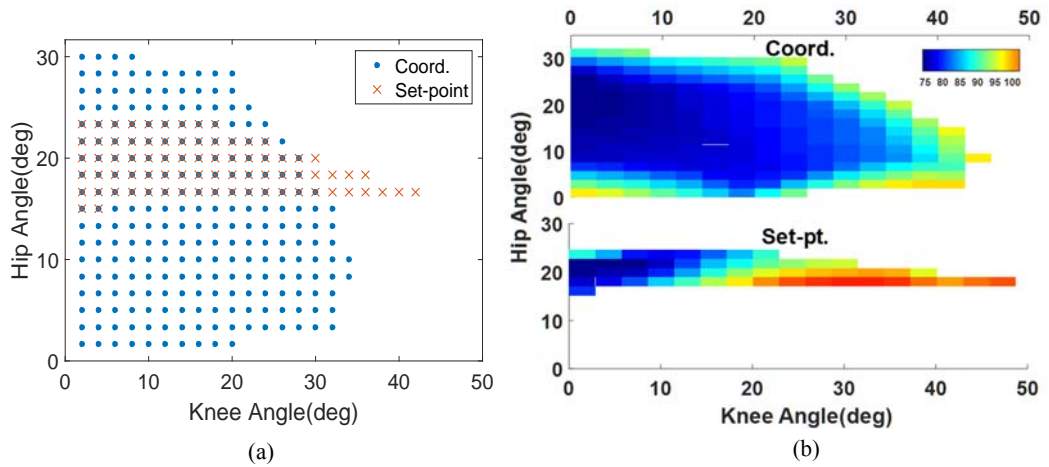


Figure 10: a) An example of the range of tolerable gait deviations under the influence of Set-point controller (orange crosses) and of coordination controller (blue dots). The nominal joint angles are indicated by the black circle. b) Peak joint torque profile (color bar in Nm) needed to restore nominal gaits in cases of the coordination controller (top) and set-point controller (bottom). The torque signature spans across tolerable range of gait deviations of knee (x axis) and hip (y axis) of the assisted side.

strategies. Driven by a bilateral strategy, the model is more sensitive to the push-off effort on the unassisted side. In Figure 11a, push-off impulses of the same magnitude are introduced to the model at the unassisted-leg liftoff (UL) after the fifth step, which results in an immediate surge in speed of the unassisted side in both controller cases. On the other hand, the assisted sides demonstrated different responses to the effort of the unassisted side to modulate speed. The assisted side of the coordination-driven model increases its speed accordingly, while the model driven by set-point control is reluctant to do the same.

The differences in ability to modulate speed lie in the different coping mechanism to changes in cadence as the result of the control strategies. The model driven by either controller is propelled by push-off impulse at unassisted-leg liftoff. The unassisted side gains speed as a result of the increasing cadence (Figure 11b). The assisted side whose cadence is coupled with the unassisted side due to interlimb

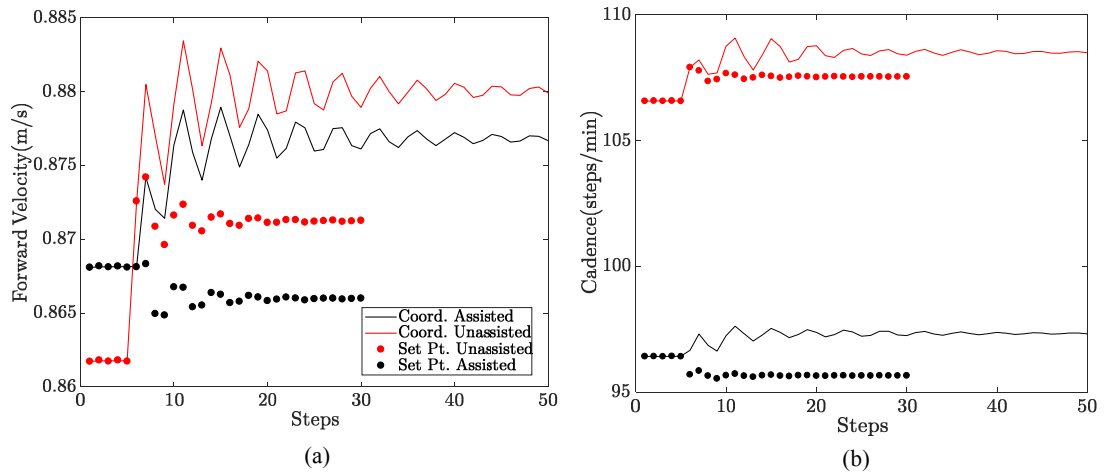


Figure 11: a) An example of evolutions of hip forward velocities over the assisted-leg swing (black) and unassisted-leg swing (red). The model driven by set-point controller (dots) and coordination controller (line) adapts to push-off impulse. b) The cadence of the unassisted sides (red) and assisted sides (black) driven by coordination controller (line) and set-point controller (dots) in response to push-off impulse.

coordination, is forced to catch up with the unassisted side by design. On the contrary, the model driven by set-point controller is unresponsive to changes in cadence, and hence the overall speed of the assisted side remains unchanged. Therefore, the model driven by the coordination strategy overall reaches a faster steady-state speed compared to the set-point control.

The model performance of speed modulation with respect to the push-off impulse under the influence of the coordination strategy scales up with the increasing magnitude of impulse. Stronger push-off effort leads larger overall gait speed (Figure 12). In contrast, the set-point controller shows a sluggish response given the same intensity of push-off impulses. The changes in speed administered by set-point controller are marginal compared to its coordination-driven counterpart. The increase in speed due to bilateral coupling is three times that of the set-point controller, and this

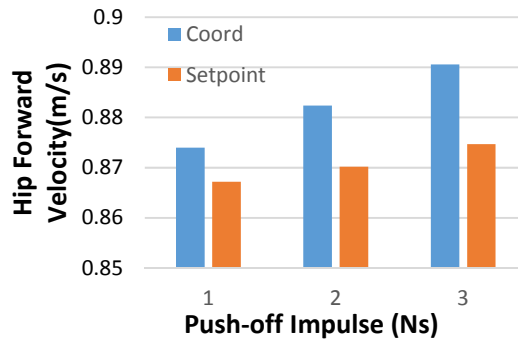


Figure 12: Hip forward velocity of the model in response to push-off impulse applied at the unassisted side liftoff (UL). The terminal speed of model driven by Coordination Strategy (blue) and Set-point Control (orange)

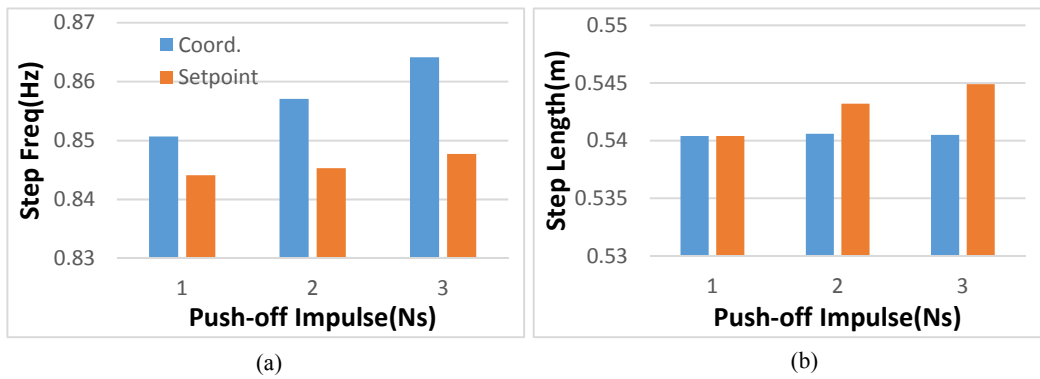


Figure 13: a) Average step frequency over 50 steps due to varying intensities of push-offs under different control strategies. b) Final step lengths in relation to the magnitude of push-off impulse under influence of different controllers.

substantial difference in response to speed modulation due to control strategies is present across all tolerable magnitudes of impulse.

For a closer look at the benefits of interlimb coordination in speed modulation, we plot the average step length and average step frequency, the two driving factors for modulating walking speed, over the period of 50 steps after the introduction of push-off impulses. The model driven by interlimb coordination, gains a faster cadence on the unassisted side as the direct results of the impulses. Its assisted side, whose cadence is

coupled with the unassisted side due to interlimb coordination, is forced to catch up with the unassisted side by design. The overall effects of the bilateral coupling result in an increase in step frequency (Figure 13a) and shows no change in step length (Figure 13b). Conversely, the set-point controller, which operates by following local point of reference, is insensitive to changes in global gait progression. Therefore, when the unassisted side modulates speed it must rely on change in step length to achieve speed modulation.

4.4 Experimental Validation

The power of the model driven by interlimb coordination to replicate the key characteristics of the human gaits not only lies in capturing nominal walking, but the coordination strategy is evident in walking gaits at a range of speeds. The evolution of the hip joint on the assisted side at numerous speeds against unassisted side single stance, normalized by the gait progression of angle θ , agree with the model in the mid/late stance (40-100%), shown in Figure 14. Despite of differences in joint kinematics and kinetics due to increased walking speeds, the differences in geometric coupling between the assisted side and unassisted side remain insignificant.

The underlying mechanism to achieve speed modulation using bilateral coordination are also observed from gait evaluation of treadmill walking. The changes of walking speeds due to push-off impulses from the simulated results and experimental data are shown in Figure 15. The changes in hip forward speed in simulation (Figure 15a) are strongly correlated to the magnitudes of the push-off impulse, with R-square values exceeding 0.98 for both control schemes. Likewise, in the experiment (Figure 15b), the changes of walking speed have a significant correlation with the effective push-off impulse derived from AGRF impulses over the propulsive phase.

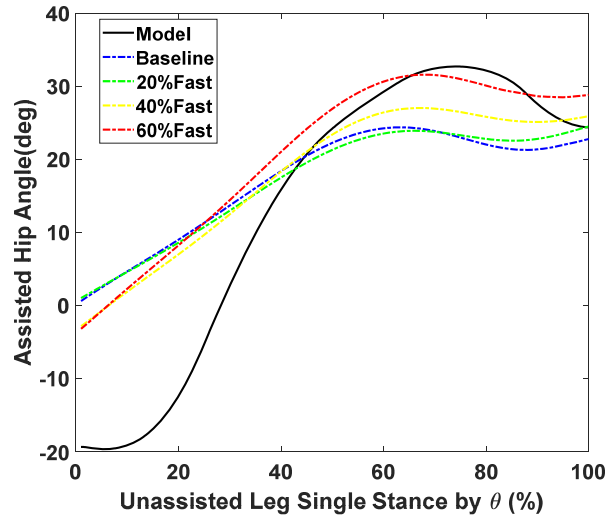


Figure 14: The geometric coupling between the assisted hip joint angles and gait progression of unassisted side indicated by are shown. Assisted hip angles of walking at numerous speeds are plotted against during the unassisted single stance

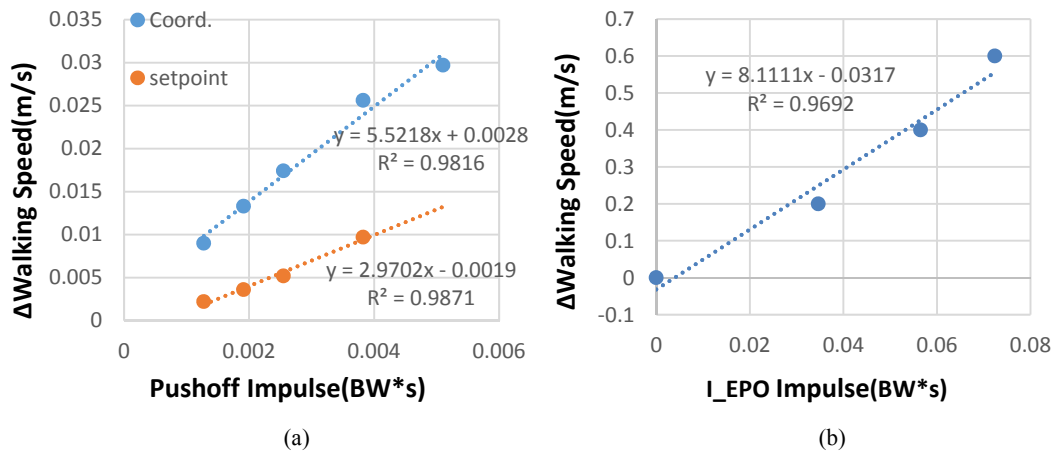


Figure 15: a) Changes in hip forward velocity due to push-off impulses (normalized by body weight) driven by interlimb coordination (blue) and set-point control (orange). b) Changes in walking speeds in response to changes in effective push-off impulses (normalized by body weight) over propulsive phase

Chapter 5

DISCUSSION

5.1 Novelty of Model

In spite of its reductive nature, this model has the minimal setup to account for the structural and functional differences between the unassisted side and the assisted side. The D-SLIP model abstracts both legs as massless springs, and it has been successful in describing the general characteristics exhibited in bipedal locomotion such as gait cycles, oscillation of CoM and conservation of energy [52]. Though it is sufficient in realizing *passive* bipedal walking gaits, it has inherent deficiencies in delineating the joint torques that are required to repeat gait cycles due to its lack of actuating components in the model. The model we proposed in this work represents the assisted side as a segmented leg model with active joint actuators during the swing phase. As a result, it enables us to quantify and articulate the amount of effort needed by the assisted and unassisted sides to move the limbs forward. Also, by segmenting the limb during swing phase, the model is allowed to achieve a multi-joint profile resembling the natural human walking (Figure 9a) that D-SLIP was not able to. However, our model still preserves the properties of energy conservation existed in D-SLIP model during stance phase due to leg compliance [52]. As it can be seen in Figure 9b, the simulated GRF profile follows a common M-shape as the GRF profile from experiments.

In addition, the intention to modulate walking speed is characterized by abstracting the additional push-off effort as an instantaneous impulse along the leg direction. It is assumed that the unassisted side would initiate the push-off effort as the motor function of the unassisted side plays a dominant role in stroke survivors. The

range of push-off impulse intensity in Figure 15 simulated in the model agrees with current studies that look at quantifying the push-off effort [53].

5.2 Significance of Interlimb Coordination

Parametrizing the interlimb coordination in a phase-dependent manner is embedded in the formulation of bipedal locomotion [54]–[56]. Such phase-dependent coordination was proven to be an intrinsic and robust approach to control limb segments to compensate for a variety of walking gaits and external disturbances [57]–[59]. A reliable phase variable candidate must possess specific characteristics, including being monotonic and unactuated. Monotonicity over time helps determine precisely where controlled joints should be at along one gait cycle. Under-actuation makes it very flexible to couple or decouple the evolution of the controlled joints with the uncontrolled degrees of freedom. The notion of creating phase-dependent joint motions has succeeded in the control of biped robots [43], [60]–[62] and the control of prosthetic devices [63], [64].

The phase-dependent interlimb coordination is shown to be present in a healthy subject by extracting the coordination pattern between joint angles of the assisted side and the phase variable θ during the assisted-leg swing (Figure 14). The solid line indicating the phase coupling in simulation showed a similar shape and matched with the trend of its experimental counterparts at mid/late stance. The discrepancy between the simulated and experimental coordination pattern at early stance is due to the fact that the model has to overcome excessive pre-swing over-extension, which is due to the model limitations that will be explained later in Section 5.4. Moreover, the phase dependency across a variety of walking speeds from slow to fast shared similar trends, despite distinct kinematic and kinetic characteristics displayed at different speeds. The

phase-driven movement patterns at the joint level was recently surveyed as an attempt to search candidate phase variables for an unifying control scheme for prosthetics, and the same results on the bilateral coordination patterns throughout the speed spectrum were reported in [55].

The phase-dependency between the two sides during swing phase evidently can be exploited to train the subjects with new interlimb coordination patterns to improve gait functions. Reisman et al. [65] suggested that interlimb coordination patterns of healthy adult subjects can be re-shaped and retained after short bouts of gait training on split-belt treadmill. Not only healthy subjects, but also subjects with chronic stroke showed significant improvements in bilateral phase-coupling and gait functions after body-weight supported treadmill training (BWSTT) [66].

5.3 Implications of Interlimb Coordination to Gait-training

As it was shown previously, a coordination-based gait-training schemes have the potential to improve the overall walking ability post-stroke by promoting a more efficient and versatile strategy. This work has shown that a bipedal walking model driven by a bilateral coordination strategy can systematically replicate human walking gaits with crucial features such as joint torques, joint motion profile and ground reaction forces. In comparison to incumbent control strategies adopted by multiple robotic gait-training platforms like [24], [47], [48], which was simulated as the set-point control in the model, the coordination-centric gait-training strategy is a more robust strategy for subjects because it can accommodate for a much larger degrees of gait deviations (Figure 10a).

Additionally, the bilateral coordination strategy enjoyed substantial advantages in energetic efficiency in recovering from gait deviations. As it is shown in Figure 10b,

the coordination strategy utilized a smaller torque to overcome the same amount of gait deviation compared to the set-point control. This suggests that the coordination-based strategy is better suited for gait-training schemes where specific bilateral coordination patterns are an integral part of the desired walking, as the embedded phase coupling automatically drives the subjects to the walking patterns with significantly improved gait energetics compared to set-point controller. The torques needed in nominal walking are slightly higher than human physiological torque during self-selected walking reported in [51]. The difference can be explained by the control actions that kick in when deviations are present, and these values agree with the magnitudes reported in earlier work [67], [68].

Furthermore, the proposed interlimb coordination strategy demonstrated significant advantages in gait adaptations and compensations to external stimuli compared to the alternative set-point control method. Its versatility is fully demonstrated in the case of speed modulation initiated by subjects' unassisted side. Unlike set-point controllers relying on local path tracking, the coordination strategy orchestrated the joint motions of the assisted side according to the progression of the gait dictated by the unassisted side. It is, by construction, positioned to monitor changes demanded by the unassisted side and it will respond to it according to the intrinsic coordination pattern. When the subject's unassisted side starts to push off harder, it causes an increase in speed of the unassisted side in either controller case (Figure 11a). The differences in ability to modulate speed lie in the different coping mechanism to changes in phase progression as the result of the control strategies (Figure 11b). The unassisted side gains speed as a result of the increasing cadence or faster phase progression. The assisted side actuated by phase coupling is bound to catch up with the unassisted side by increasing

its cadence. On the contrary, the model driven by the set-point controller is unresponsive to changes in cadence, and hence the overall speed of the assisted side remains unchanged. Therefore, the model driven by the coordination strategy overall reaches a faster steady-state speed compared to the set-point control.

Governed by the coordination pattern described in section 2.3.2, the subject is adept to take advantage of one single pattern to effectively modulate to a variety of walking speeds by voluntarily modifying the cadence of the unassisted side. The effectiveness of bilateral coordination is even more outstanding as the magnitude of the impulses increases. The overall effects of the bilateral coupling result in an increase in step frequency (Figure 12a) and show no change in step length (Figure 12b). Conversely, the set-point controller, which operates by following a local point of reference, is insensitive to changes in global gait progression. Therefore, when the unassisted side modulates the speed, the assisted side must rely on changes in step length to achieve speed modulation. This has important implications for gait-rehabilitation, as both strategies for speed modulations (step length vs step frequency) have been observed in the stroke population during rehabilitation [14], [34], [69].

5.4 Limitations

One of the primary limitations of this work, as mentioned in Chapter 1, is that this model does not discriminate the effort by the subject from the effort by robotic gait-trainers, functional electrical stimulation, or other means to intervene; but it rather considers the combined effort to achieve the desired walking gaits. The results from the simulation cannot be directly applied to gait-training in the clinical setting, as this model does not capture how the subject interacts with the external assistance and the subject's own compensatory dynamics. This work is not trying to claim that each subject is going

to respond to certain training strategies in a certain way, rather it aims at offering a framework that allows for prescribing the collaborative effort of the combined system as a whole, as well as visualize the effects of the designated control actions on the gait performance in a simulated setting.

Similar to other reductive models mentioned in [38], [43], the model is inherently limited to fully replicate all aspects of human locomotion due to its existing infrastructure. The simulated walking gaits exhibited a late hip and knee extension, which is due to the lack of an ankle-foot segment in the model. Without modelling the ankle-foot plantarflexion which is essential to swing initiation, forward progression [70], energy reduction [71] and necessary for gait aesthetics, the hip and knee joints have to compensate by over-extending during the late stance as it can be seen in Figure 9a. As a result, both hip and knee joints reach the peak flexion angles at a later time because they have to overcome the excessive joint extensions.

In addition, the push-off effort by the unassisted side is abstracted by an instantaneous impulse along the leg at the instance of lift-off. This does not truly represent the propulsion efforts produced by ankle-foot plantar-flexors. A continuous input of push-off force over the period of propulsion would be a closer characterization of the push-off effort. Furthermore, studies have indicated that the trailing limb angle at the end of push-off phase is a major contributing factor to the effectiveness of push-off [72], which our model and experimental data do not particularly take into consideration.

The foundation of the geometric coupling is the parametrization of joint pattern with respect to a monotonic phase variable θ . This limits certain motions such as back-stepping which will result in an evolution of θ in the backward direction. Moreover, the geometric coupling as a result of interlimb coordination isolates the effect of changes in

cadence or step frequency on speed modulation. Yet, studies have shown that both changes in cadence and step length contribute to modulating the speed in able-bodied subjects [73], [74]. However there are studies that point out that stroke subjects tend to prefer walking with a higher cadence rather than longer step length [75]. The current control strategy is limited by its ability to accommodate speed changes due to changes in the step length, which leaves the door open for future work to encourage modified control strategies that allow for variability of step length.

Chapter 6

CONCLUSIONS AND FUTURE WORK

6.1 Conclusions

A variety of reductive models have been introduced to study bipedal locomotion. Such models offer unifying descriptions of macroscopic-level locomotion behavior without delving into the intricacy of neuro-muscular inner workings. This thesis focused on a model for bipedal walking, with the objective to better understand the effects of coordination-centric control strategy on the gait performance in a simulated setting and explore the potency of this strategy as a feasible gait-training strategy for subjects with pathological gait.

Motivated by the D-SLIP model, we proposed a sagittal-plane model that differentiates the assisted leg - represented by a two-link segmented leg augmented by joint actuations during swing phase - from the unassisted side modelled by a SLIP. Our model was shown to be capable of realizing critical characteristics of bipedal walking gaits. The simulated walking gaits were validated with experimental data of a healthy human walking on the treadmill, and they showed close resemblance to their experimental counterparts. Moreover, the model provides direct access to manipulate individual joints and it provides the basic infrastructure for quantifying the joint torque individually or collaboratively to accomplish desired walking gaits.

Inspired by the underlying mechanism of bipedal locomotion, a bilateral control strategy that is based on interlimb geometric coupling, was used to prescribe the joint motions in this model template. Alongside with the existing alternative strategy (set-point controller) that is widely adopted in robotic gait-training schemes, the bilateral strategy was evaluated in simulated experiments to demonstrate its performance in

disturbance rejection. The bilateral strategy outperformed the alternative strategy in gait energetic costs and robustness.

Another aspect that was examined in this work was the response of the proposed interlimb coordination strategy with respect to push-off to modulate the model's walking speeds. In comparison with the alternative strategy that emphasizes local path tracking, it is shown that the geometric coupling embedded in interlimb coordination is much more effective in adapting the walking speeds. Furthermore, similar coordination patterns are observed in the treadmill walking experiments from normal to fast speeds conducted on healthy subjects, and this shows that this bilateral strategy is partially responsible for the speed modulation in the clinical setting.

6.2 Future Work

6.2.1 Model Framework

This work has so far primarily focused on characterizing the nominal walking gaits and the model has demonstrated its success with gait experiments of the healthy subject. It is yet to be investigated whether the proposed model framework can realize the pathological gaits.

The varying degrees of impairments in post-stroke individuals pose a fundamental challenge to characterizing the asymmetric gaits using a unified model like the one proposed in this work. It still remains an open research question that what common characteristics and features among the pathological cases would better be realized from such model. One of the benefits of having such a reduced-order model framework is that it allows us to compartmentalize different aspects of the pathological cases and investigate the effects of interventions by evaluating the corresponding

performance. The current framework sets the stage for discerning the characteristics of joint motions simply by different phases during the gait cycle. One way to evaluate the performance of the model in pathological gaits is to compare the joint torques from simulation during the swing phase with the experimental data, by feeding the joint profile of subjects recorded from gait evaluation experiment outlined in Section 3.3 into the model as the initial guess for the parameter optimization scheme described in Section 2.3.3, where the profile matching will be taken into account by the objective function. This way, the periodic walking gaits (fixed points) concerning the pathological cases can be first established, and then therapists can modify different aspects of the motion such as the coordination pattern, push-off impulses and etc. to evaluate their effects on the subjects.

The other aspect of the model framework that is still open to further studies is to close the loop on control schemes for the assisted-leg during its stance phase. The stance phase is critical for locomotive tasks such as body support, swing-initiation and energetic costs. In addition, it has been demonstrated in D-SLIP models that the leg compliance is the key to achieving natural walking kinematics and comparable energetic characteristics. There are studies in robotics and prosthetics utilizing the impedance control regime [76], [77] via virtual constraints to regulate the stance phase.

6.2.2 Experimental Validation

The natural next step is to implement the bilateral coordination strategy developed in Chapter 2.3.1 on a robotic gait-training platform (Figure 16) to evaluate its effectiveness in the clinical setting. It would be beneficial to formulate a training scheme centered around the bilateral strategy in contrast to control groups using the existing gait-training paradigm.



Figure 16: Active-leg Exoskeleton (ALEX) robotic platform for post-stroke gait-training

REFERENCES

- [1] D. A. Winter and P. Eng, “Kinetics: our window into the goals and strategies of the central nervous system,” *Behav. Brain Res.*, vol. 67, no. 2, pp. 111–120, Mar. 1995.
- [2] S. Grillner and P. Zangger, “On the central generation of locomotion in the low spinal cat,” *Exp. Brain Res.*, vol. 34, no. 2, Jan. 1979.
- [3] A. J. Ijspeert, A. Crespi, D. Ryczko, and J.-M. Cabelguen, “From swimming to walking with a salamander robot driven by a spinal cord model,” *Science*, vol. 315, no. 5817, pp. 1416–1420, 2007.
- [4] J. J. Collins and S. A. Richmond, “Hard-wired central pattern generators for quadrupedal locomotion,” *Biol. Cybern.*, vol. 71, no. 5, pp. 375–385, Sep. 1994.
- [5] M. R. Dimitrijevic, Y. Gerasimenko, and M. M. Pinter, “Evidence for a Spinal Central Pattern Generator in Humans,” *Ann. N. Y. Acad. Sci.*, vol. 860, no. 1 NEURONAL MECH, pp. 360–376, Nov. 1998.
- [6] V. Dietz, “Do human bipeds use quadrupedal coordination?,” *Trends Neurosci.*, vol. 25, no. 9, pp. 462–467, 2002.
- [7] J. Duysens and H. W. A. . Van de Crommert, “Neural control of locomotion; Part 1: The central pattern generator from cats to humans,” *Gait Posture*, vol. 7, no. 2, pp. 131–141, Mar. 1998.
- [8] N. Hogan and D. Sternad, “Dynamic primitives in the control of locomotion,” *Front. Comput. Neurosci.*, vol. 7, no. June, p. 71, 2013.
- [9] S. . P. Swinnen and R. . G. Carson, “The control and learning of patterns of interlimb coordination: Past and present issues in normal and disordered control,” *Acta Psychol. (Amst.)*, vol. 110, no. 2–3, pp. 129–137, Jun. 2002.
- [10] E. P. Zehr, J. E. Balter, D. P. Ferris, S. R. Hundza, P. M. Loadman, and R. H. Stoloff, “Neural regulation of rhythmic arm and leg movement is conserved across human locomotor tasks,” *J. Physiol.*, vol. 582, no. 1, pp. 209–227, Jul. 2007.
- [11] R. Jung, A. Belanger, T. Kanchiku, M. Fairchild, and J. J. Abbas, “Neuromuscular stimulation therapy after incomplete spinal cord injury promotes recovery of interlimb coordination during locomotion,” *J. Neural Eng.*, vol. 6, no. 5, p. 055010, Oct. 2009.
- [12] D. Mozaffarian, E. J. Benjamin, A. S. Go, D. K. Arnett, M. J. Blaha, M. Cushman, S. de Ferranti, J.-P. Després, H. J. Fullerton, V. J. Howard, M. D. Huffman, S. E. Judd, B. M. Kissela, D. T. Lackland, J. H. Lichtman, L. D. Lisabeth, S. Liu, R. H. Mackey, D. B. Matchar, D. K. McGuire, E. R. Mohler, C. S. Moy, P. Muntner, M. E. Mussolino, K. Nasir, R. W. Neumar, G. Nichol, L. Palaniappan, D. K. Pandey, M. J. Reeves, C. J. Rodriguez, P. D. Sorlie, J. Stein, A. Towfighi, T. N. Turan, S. S. Virani, J. Z. Willey, D. Woo, R. W. Yeh, and M. B. Turner, “Heart Disease and Stroke Statistics-2015 Update: A Report From the American Heart Association,” *Circulation*, vol. 131, no. 4, pp. e29–322, Dec. 2014.

- [13] V. Dietz and W. Berger, "Interlimb coordination of posture in patients with spastic paresis: Impaired function of spinal reflexes," *Brain*, vol. 107, no. 3, pp. 965–978, Sep. 1984.
- [14] M. Roerdink, C. J. C. Lamoth, G. Kwakkel, P. C. W. van Wieringen, and P. J. Beek, "Gait coordination after stroke: benefits of acoustically paced treadmill walking.," *Phys. Ther.*, vol. 87, no. 8, pp. 1009–22, Aug. 2007.
- [15] C.-Y. Wu, S.-H. Chou, C.-L. Chen, M.-Y. Kuo, T.-W. Lu, and Y.-C. Fu, "Kinematic analysis of a functional and sequential bimanual task in patients with left hemiparesis: intra-limb and interlimb coordination," *Disabil. Rehabil.*, vol. 31, no. 12, pp. 958–966, Jan. 2009.
- [16] M. G. Bowden, C. K. Balasubramanian, R. R. Neptune, and S. A. Kautz, "Anterior-posterior ground reaction forces as a measure of paretic leg contribution in hemiparetic walking," *Stroke*, vol. 37, no. 3, pp. 872–876, 2006.
- [17] G. Chen, C. Patten, D. H. Kothari, and F. E. Zajac, "Gait differences between individuals with post-stroke hemiparesis and non-disabled controls at matched speeds," *Gait Posture*, vol. 22, no. 1, pp. 57–62, 2005.
- [18] S. Nadeau, D. Gravel, A. B. Arseneault, and D. Bourbonnais, "Plantarflexor weakness as a limiting factor of gait speed in stroke subjects and the compensating role of hip flexors," *Clin Biomech (Bristol, Avon)*, vol. 14, no. 2, p. 125–35., 1999.
- [19] S. J. Olney, M. P. Griffin, and I. D. McBride, "Temporal, kinematic, and kinetic variables related to gait speed in subjects with hemiplegia: a regression approach," *Phys Ther*, vol. 74, no. 9, p. 872–85., 1994.
- [20] S. J. Olney and C. Richards, "Hemiparetic gait following stroke. Part I: Characteristics," *Gait Posture*, vol. 4, pp. 136–148, 1996.
- [21] K. K. Patterson, I. Parafianowicz, C. J. Danells, V. Closson, M. C. Verrier, W. R. Staines, S. E. Black, and W. E. McIlroy, "Gait asymmetry in community-ambulating stroke survivors.," *Arch. Phys. Med. Rehabil.*, vol. 89, no. 2, pp. 304–10, Feb. 2008.
- [22] S. E. Lord, K. McPherson, H. K. McNaughton, L. Rochester, and M. Weatherall, "Community ambulation after stroke: how important and obtainable is it and what measures appear predictive?," *Arch. Phys. Med. Rehabil.*, vol. 85, no. 2, pp. 234–9, Feb. 2004.
- [23] S. E. Lord and L. Rochester, "Measurement of community ambulation after stroke: current status and future developments.," *Stroke.*, vol. 36, no. 7, pp. 1457–61, Jul. 2005.
- [24] S. K. Banala, S. H. Kim, S. K. Agrawal, and J. P. Scholz, "Robot Assisted Gait Training With Active Leg Exoskeleton (ALEX)," *IEEE Trans. neural Syst. Rehabil. Eng.*, vol. 17, no. 1, pp. 2–8, 2009.
- [25] P.-C. Kao, S. Srivastava, S. K. Agrawal, and J. P. Scholz, "Effect of robotic performance-based error-augmentation versus error-reduction training on the gait of healthy individuals.," *Gait Posture*, vol. 37, no. 1, pp. 113–20, Jan. 2013.

- [26] M. Wu, J. M. Landry, J. Kim, B. D. Schmit, S.-C. Yen, and J. Macdonald, "Robotic resistance/assistance training improves locomotor function in individuals poststroke: a randomized controlled study.," *Arch. Phys. Med. Rehabil.*, vol. 95, no. 5, pp. 799–806, May 2014.
- [27] J. Hidler, D. Nichols, M. Pelliccio, K. Brady, D. D. Campbell, J. H. Kahn, and T. G. Hornby, "Multicenter randomized clinical trial evaluating the effectiveness of the Lokomat in subacute stroke.," *Neurorehabil. Neural Repair*, vol. 23, no. 1, pp. 5–13, 2009.
- [28] B. Husemann, F. Müller, C. Krewer, S. Heller, and E. Koenig, "Effects of locomotion training with assistance of a robot-driven gait orthosis in hemiparetic patients after stroke: A randomized controlled pilot study," *Stroke*, vol. 38, no. 2, pp. 349–354, 2007.
- [29] S. Srivastava, "The Effects of Gait Retraining on Muscle Coordination and Functional Walking Ability Post-stroke," 2014.
- [30] S. H. Kim, S. K. Banala, E. a. Brackbill, S. K. Agrawal, V. Krishnamoorthy, and J. P. Scholz, "Robot-assisted modifications of gait in healthy individuals," *Exp. Brain Res.*, vol. 202, no. 4, pp. 809–824, 2010.
- [31] J. Skidmore and P. Artemiadis, "On the effect of walking surface stiffness on inter-limb coordination in human walking: Toward bilaterally informed robotic gait rehabilitation," *J. Neuroeng. Rehabil.*, vol. 13, no. 1, p. 32, Dec. 2016.
- [32] H. Vallery, E. H. F. van Asseldonk, M. Buss, and H. van der Kooij, "Reference trajectory generation for rehabilitation robots: complementary limb motion estimation.," *IEEE Trans. Neural Syst. Rehabil. Eng.*, vol. 17, no. 1, pp. 23–30, Feb. 2009.
- [33] S. Seiterle, T. Susko, P. K. Artemiadis, R. Riener, and H. Igo Krebs, "Interlimb coordination in body-weight supported locomotion: A pilot study," *J. Biomech.*, vol. 48, no. 11, pp. 2837–2843, Aug. 2015.
- [34] D. S. Reisman, R. Wityk, K. Silver, and A. J. Bastian, "Split-belt treadmill adaptation transfers to overground walking in persons poststroke.," *Neurorehabil. Neural Repair*, vol. 23, no. 7, pp. 735–44, Sep. 2009.
- [35] D. G. Thelen, F. C. Anderson, and S. L. Delp, "Generating dynamic simulations of movement using computed muscle control," *J. Biomech.*, vol. 36, no. 3, pp. 321–328, Mar. 2003.
- [36] F. C. Anderson and M. G. Pandy, "Dynamic optimization of human walking.," *J. Biomech. Eng.*, vol. 123, no. October, pp. 381–390, 2001.
- [37] R. J. Full and D. E. Koditschek, "Templates and anchors: neuromechanical hypotheses of legged locomotion on land.," *J. Exp. Biol.*, vol. 202, no. Pt 23, pp. 3325–3332, 1999.
- [38] H. Geyer, A. Seyfarth, and R. Blickhan, "Compliant leg behaviour explains basic dynamics of walking and running.," *Proc. Biol. Sci.*, vol. 273, no. November, pp. 2861–2867, 2006.
- [39] C. K. Jung and S. Park, "Compliant bipedal model with the center of pressure excursion associated with oscillatory behavior of the center of mass reproduces

- the human gait dynamics,” *J. Biomech.*, vol. 47, no. 1, pp. 223–229, Jan. 2014.
- [40] S. Kim and S. Park, “Leg stiffness increases with speed to modulate gait frequency and propulsion energy,” *J. Biomech.*, vol. 44, no. 7, pp. 1253–1258, Apr. 2011.
- [41] C. E. Mahon, D. J. Farris, G. S. Sawicki, and M. D. Lewek, “Individual limb mechanical analysis of gait following stroke,” *J. Biomech.*, vol. 48, no. 6, pp. 984–9, Apr. 2015.
- [42] D. Wei, I. Poulakakis, and J. Higginson, “Human-Exoskeleton Hybrid Model to Produce Stable Gait through Inter-limb Coordination,” *archive.asbweb.org*, 2015.
- [43] E. Westervelt, J. J. W. Grizzle, C. Chevallereau, H. C. Jun, and B. Morris, *Feedback Control of Dynamic Bipedal Robot Locomotion*. CRC Press, 2007.
- [44] Y. Hurmuzlu and D. B. Marghitu, “Rigid Body Collisions of Planar Kinematic Chains With Multiple Contact Points,” *Int. J. Rob. Res.*, vol. 13, no. 1, pp. 82–92, Feb. 1994.
- [45] E. Westervelt, J. Grizzle, and C. Chevallereau, *Feedback control of dynamic bipedal robot locomotion*. 2007.
- [46] J. Guckenheimer and P. Holmes, *Nonlinear Oscillations, Dynamical Systems, and Bifurcations of Vector Fields*. Springer Science & Business Media, 1983.
- [47] S. Jezernik, G. Colombo, T. Keller, H. Frueh, and M. Morari, “Robotic Orthosis Lokomat: A Research and Rehabilitation Tool,” *Neuromodulation*, vol. 6, no. 2, pp. 108–115, 2003.
- [48] D. Zanotto, P. Stegall, and S. Agrawal, “ALEX III: A Novel Robotic Platform for Gait Training - Design of the 4-DOF Leg,” *IEEE Intl. Conf. Robot. Autom.*, pp. 3914–3919, 2013.
- [49] S. Banala, A. Kulpe, and S. Agrawal, “A powered leg orthosis for gait rehabilitation of motor-impaired patients,” *Robot. Autom. ...*, 2007.
- [50] D. A. Winter, *Biomechanics and motor control of human movement*. Wiley, 2009.
- [51] P. DeVita and T. Hortobagyi, “Age causes a redistribution of joint torques and powers during gait,” *J. Appl. Physiol.*, vol. 88, no. 5, pp. 1804–1811, 2000.
- [52] J. Rummel, Y. Blum, H. M. Maus, C. Rode, and A. Seyfarth, “Stable and robust walking with compliant legs,” *Proc. - IEEE Int. Conf. Robot. Autom.*, pp. 5250–5255, 2010.
- [53] H. Y. Hsiao, T. M. Zabielski, J. A. Palmer, J. S. Higginson, and S. A. Binder-Macleod, “Evaluation of measurements of propulsion used to reflect changes in walking speed in individuals poststroke,” *J. Biomech.*, vol. 49, no. 16, pp. 4107–4112, Dec. 2016.
- [54] G. Taga, “A model of the neuro-musculo-skeletal system for human locomotion,” *Biol. Cybern.*, vol. 73, no. 2, pp. 97–111, Jul. 1995.
- [55] D. Villarreal and R. Gregg, “A Survey of Phase Variable Candidates of Human Locomotion,” *IEEE Eng. Med. Biol. Soc.*, pp. 2–6, 2014.
- [56] R. Grasso, L. Bianchi, and F. Lacquaniti, “Motor Patterns for Human Gait:

- Backward Versus Forward Locomotion,” *J. Neurophysiol.*, vol. 80, no. 4, pp. 1868–1885, Oct. 1998.
- [57] H. Forssberg, “Stumbling corrective reaction: a phase-dependent compensatory reaction during locomotion.,” *J. Neurophysiol.*, vol. 42, no. 4, pp. 936–53, Jul. 1979.
- [58] V. Dietz, J. Quintern, G. Boos, and W. Berger, “Obstruction of the swing phase during gait: phase-dependent bilateral leg muscle coordination,” *Brain Res.*, vol. 384, no. 1, pp. 166–169, Oct. 1986.
- [59] P. K. Artemiadis and H. I. Krebs, “Interlimb coordination evoked by unilateral mechanical perturbation during body-weight supported gait,” *IEEE Int. Conf. Rehabil. Robot.*, 2011.
- [60] K. Sreenath, H.-W. Park, I. Poulakakis, and J. W. Grizzle, “A Compliant Hybrid Zero Dynamics Controller for Stable, Efficient and Fast Bipedal Walking on MABEL,” *Int. J. Rob. Res.*, vol. 30, no. 9, pp. 1170–1193, Sep. 2011.
- [61] A. Ramezani, J. W. Hurst, K. Akbari Hamed, and J. W. Grizzle, “Performance Analysis and Feedback Control of ATRIAS, A Three-Dimensional Bipedal Robot,” *J. Dyn. Syst. Meas. Control*, vol. 136, no. 2, p. 021012, Dec. 2013.
- [62] M. J. Powell, H. Zhao, and A. D. Ames, “Motion primitives for human-inspired bipedal robotic locomotion: walking and stair climbing,” in *2012 IEEE International Conference on Robotics and Automation*, 2012, pp. 543–549.
- [63] M. a Holgate, T. G. Sugar, and W. B. Alexander, “A Novel Control Algorithm for Wearable Robotics using Phase Plane Invariants,” *2009 IEEE Int. Conf. Robot. Autom.*, pp. 3845–3850, May 2009.
- [64] D. Quintero, A. E. Martin, and R. D. Gregg, “Unifying the Gait Cycle in the Control of a Powered Prosthetic Leg,” pp. 2–7.
- [65] D. S. Reisman, H. J. Block, and A. J. Bastian, “Interlimb coordination during locomotion: what can be adapted and stored?,” *J. Neurophysiol.*, vol. 94, no. 4, pp. 2403–2415, 2005.
- [66] S. A. Combs, E. L. Dugan, E. N. Ozimek, and A. B. Curtis, “Bilateral coordination and gait symmetry after body-weight supported treadmill training for persons with chronic stroke,” *Clin. Biomech.*, vol. 28, no. 4, pp. 448–453, Apr. 2013.
- [67] A. Duschau-Wicke, J. Von Zitzewitz, A. Caprez, L. Lünenburger, and R. Riener, “Path control: A method for patient-cooperative robot-aided gait rehabilitation,” *IEEE Trans. Neural Syst. Rehabil. Eng.*, vol. 18, no. 1, pp. 38–48, 2010.
- [68] S. K. Banala, S. K. Agrawal, A. Fattah, V. Krishnamoorthy, W. L. Hsu, J. Scholz, and K. Rudolph, “Gravity-balancing leg orthosis and its performance evaluation,” *IEEE Trans. Robot.*, vol. 22, no. 6, pp. 1228–1239, 2006.
- [69] M. . Thaut, G. . McIntosh, and R. . Rice, “Rhythmic facilitation of gait training in hemiparetic stroke rehabilitation,” *J. Neurol. Sci.*, vol. 151, no. 2, pp. 207–212, Oct. 1997.

- [70] R. R. Neptune, S. A. Kautz, and F. E. Zajac, "Contributions of the individual ankle plantar flexors to support, forward progression and swing initiation during walking," *J. Biomech.*, vol. 34, no. 11, pp. 1387–1398, Nov. 2001.
- [71] A. D. Kuo, "Energetics of actively powered locomotion using the simplest walking model.," *J. Biomech. Eng.*, vol. 124, no. 1, pp. 113–120, 2002.
- [72] H. Hsiao, B. A. Knarr, J. S. Higginson, and S. A. Binder-Macleod, "Mechanisms to increase propulsive force for individuals poststroke.," *J. Neuroeng. Rehabil.*, vol. 12, no. 1, p. 40, Jan. 2015.
- [73] M. S. Orendurff, G. C. Bernatz, J. A. Schoen, and G. K. Klute, "Kinetic mechanisms to alter walking speed," *Gait Posture*, vol. 27, no. 4, pp. 603–610, May 2008.
- [74] M. P. Murray, L. a Mollinger, G. M. Gardner, and S. B. Sepic, "Kinematic and EMG patterns during slow, free, and fast walking.," *J. Orthop. Res.*, vol. 2, no. 3, pp. 272–280, 1984.
- [75] J. Jonsdottir, M. Recalcati, M. Rabuffetti, A. Casiraghi, S. Boccardi, and M. Ferrarin, "Functional resources to increase gait speed in people with stroke: Strategies adopted compared to healthy controls," *Gait Posture*, vol. 29, no. 3, pp. 355–359, Apr. 2009.
- [76] F. Sup, a. Bohara, and M. Goldfarb, "Design and Control of a Powered Transfemoral Prosthesis," *Int. J. Rob. Res.*, vol. 27, no. 2, pp. 263–273, 2008.
- [77] N. Aghasadeghi, Huihua Zhao, L. J. Hargrove, A. D. Ames, E. J. Perreault, and T. Bretl, "Learning impedance controller parameters for lower-limb prostheses," in *2013 IEEE/RSJ International Conference on Intelligent Robots and Systems*, 2013, pp. 4268–4274.